1 **Re-programming of GM-CSF-dependent alveolar macrophages through GSK3 activity modulation**

2

3 Israel Ríos[1], Cristina Herrero[1], Mónica Torres-Torresano[2], Baltasar López-Navarro[2], María Teresa
4 Schiaffino[2], Francisco Díaz-Crespo[3], Alicia Nieto-Valle[4], Rafael Samaniego[4], Yolanda Sierra-
5 Palomares[5], Eduardo Oliver[5], Fernando Revuelta-Salgado[6], Ricardo García-Luján[6], Paloma Sánchez-
6 Mateos[4,7], Rafael Delgado[8,9], Amaya Puig-Kröger[2#*] , Ángel L. Corbí[1#*].

7

8 [1] Myeloid Cell Laboratory, Centro de Investigaciones Biológicas, CSIC, Madrid, Spain.
9 [2] Unidad de Inmuno-Metabolismo e Inflamación, Instituto de Investigación Sanitaria Gregorio
10 Marañón (IiSGM), Hospital General Universitario Gregorio Marañón, Madrid, Spain.
11 [3] Servicio de Anatomía Patológica, Hospital General Universitario Gregorio Marañón, Madrid,
12 Spain.
13 [4] Unidad de Microscopía Confocal, Instituto de Investigación Sanitaria Gregorio Marañón (IiSGM),
14 Hospital General Universitario Gregorio Marañón, Madrid, Spain.
15 [5] Experimental Pharmacology and New Tragets in Cardiopulmonary Disorders, Centro de
16 Investigaciones Biológicas, CSIC, Madrid, Spain.
17 [6] Servicio de Neumología. Hospital Universitario 12 de Octubre. Madrid, Spain.
18 [7] Department of Immunology, Ophthalmology and ENT, Universidad Complutense School of
19 Medicine, Madrid, Spain.
20 [8] Instituto de Investigación Hospital Universitario 12 de Octubre (imas12), Madrid, Spain.
21 [9] Universidad Complutense School of Medicine, Madrid, Spain.

22

23 # APK and ALC contributed equally to this work.

24

25 * Corresponding authors: Dr. Ángel L. Corbí (acorbi@cib.csic.es). Centro de Investigaciones
26 Biológicas "Margarita Salas", CSIC. Ramiro de Maeztu, 9. Madrid 28040; Phone: 34-91-8373112;
27 Dr. Amaya Puig-Kröger (amaya.puig@iisgm.com). Unidad de Inmuno-Metabolismo e Inflamación,
28 Instituto de Investigación Sanitaria Gregorio Marañón (IiSGM), Madrid, Spain. Phone: 34-91-
29 4269268.

SUMMARY

Monocyte-derived macrophages recruited into inflamed tissues can acquire an array of functional states depending on the extracellular environment. Since the anti-inflammatory/pro-fibrotic macrophage profile is determined by MAFB, whose activity/protein levels are regulated by GSK3, we addressed the macrophage re-programming potential of GSK3 modulation. GM-CSF-dependent (GM-MØ) and M-CSF-dependent monocyte-derived macrophages (M-MØ) exhibited distinct levels of inactive GSK3, and inhibiting GSK3 in GM-MØ led to acquisition of transcriptional, phenotypic and functional properties characteristic of M-MØ (enhanced expression of IL-10 and monocyte-recruiting factors, and higher efferocytosis). These re-programming effects were also observed upon GSK3α/β knockdown, and through GSK3 inhibition in *ex vivo* isolated human alveolar macrophages (AMØ). Notably, GSK3 downmodulation potentiated the transcriptional signature of Interstitial Macrophages (IMØ) while suppressed the AMØ-specific gene profile. Indeed, heightened levels of inactive GSK3 and MAFB-dependent proteins were observed in severe COVID-19 patients lung macrophages, highlighting the GSK3-MAFB axis as a therapeutic target for macrophage re-programming.

48 **INTRODUCTION**

49 Macrophages exhibit considerable functional plasticity during inflammatory responses,
50 transitioning from pro-inflammatory activities to tissue repair and inflammation resolution [1,2]. This
51 functional versatility of macrophages is intrincately tied to factors such as their ontogeny (fetal
52 origin vs. monocyte-derived) and the specific tissue and extracellular environment [3–5]. Notably,
53 monocyte-derived macrophages are oppositely instructed by M-CSF or GM-CSF [6–12]. GM-CSF
54 directs monocyte-derived macrophages (GM-MØ) towards heightened pro-inflammatory activity
55 [10,13–15] and the acquisition of the lung alveolar macrophage phenotype and gene profile [16]. In fact,
56 GM-CSF is essential for generating lung alveolar macrophages [17], crucial for surfactant
57 homeostasis, whereas deficient GM-CSF signaling leads to pulmonary alveolar proteinosis [18], a
58 condition marked by defective surfactant clearance and disruption of pulmonary homeostasis due
59 to alveolar macrophage dysfunction [19]. Conversely, M-CSF gives rise to anti-inflammatory, pro-
60 resolving, and immunosuppressive monocyte-derived macrophages (M-MØ) [1,2,20] but promotes
61 the development of pro-fibrotic pathogenic monocyte-derived macrophages in lung pathologies
62 like idiopathic pulmonary fibrosis (IPF) [21] and severe COVID-19 [22]. The pathological relevance of
63 GM-MØ and M-MØ subsets is evident in severe COVID-19, with a huge increase in monocyte-
64 derived M-MØ and a reduction of tissue-resident GM-MØ-like lung macrophages [23–25].

65

66 Despite their crucial role in maintaining tissue homeostasis, deregulated macrophage functional
67 specialization contributes to various human diseases, including tumors and chronic inflammatory
68 pathologies [26]. Consequently, macrophage re-programming has emerged as a promising
69 therapeutic approach [26]. However, achieving this necessitates a profound understanding of the
70 transcriptional and signaling mechanisms governing the pro- and anti-inflammatory nature of
71 macrophages. In this regard, recent findings indicate that the homeostatic and reparative

72 transcriptional profile of human M-MØ is orchestrated by MAF and MAFB [27–29], closely related
73 transcription factors that regulate stemness and self-renewal in the mouse haematopoietic lineage
74 [30–35]. In fact, the distinctive expression of MAFB in M-MØ, influencing IL-10 production [27,36], also
75 mediates macrophage re-programming induced by methotrexate [37] and LXR ligands [38].
76
77 Given the pivotal role of MAFB/MAF in human macrophage functional specification, and
78 considering
79 the regulation of large MAF factors through GSK3-mediated phosphorylation-induced proteasomal
80 degradation [30], we hypothesized that modulating GSK3 activity could offer a viable avenue for re-
81 programming monocyte-derived macrophages. Our findings reveal significant differences in
82 inhibitory phosphorylation of GSK3β (Ser^9-GSK3β) and GSK3α (Ser^{21}-GSK3α) between M-MØ and
83 GM-MØ, and that GSK3 inhibition (using CHIR-99021) or knock-down (using siRNA) in GM-MØ
84 prompts the adoption of transcriptional, phenotypic, and functional characteristics resembling
85 those of M-MØ. This re-programming effect was manifested in elevated expression of IL-10,
86 monocyte-recruiting chemokines, pro-fibrotic factors, as well as in enhanced phagocytic capability,
87 all correlating with increased MAFB expression. The re-programming action of GSK3 inhibition was
88 also observed in control monocytes and in monocytes exposed to a pathological pro-inflammatory
89 environment. Importantly, GSK3 inhibition in *ex vivo* isolated human Alveolar Macrophages
90 (AMØ), led to the loss of the AMØ gene signature and the acquisition of the gene profile that
91 characterizes Interstitial Macrophages (IMØ). Since pathogenic lung macrophages in severe
92 COVID-19 exhibit high levels of inactive GSK3 and heightened levels of MAFB and MAFB-
93 dependent proteins, our results underscore the potent macrophage re-programming impact of
94 GSK3 inhibition, and highlight the GSK3-MAFB axis as a promising therapeutic target for
95 macrophage re-programming.

96 **EXPERIMENTAL PROCEDURES**

97 **Generation of human monocyte-derived macrophages *in vitro* and treatments**. Human
98 Peripheral Blood Mononuclear Cells (PBMCs) were isolated from buffy coats from anonymous
99 healthy donors over a Lymphoprep (Nycomed Pharma) gradient according to standard procedures.
100 Monocytes were purified from PBMC by magnetic cell sorting using anti-CD14 microbeads
101 (Miltenyi Biotec). Monocytes (>95% $CD14^+$ cells) were cultured at 0.5 x 10^6 cells/ml in Roswell Park
102 Memorial Institute (RPMI 1640, Gibco) medium supplemented with 10% fetal bovine serum (FBS,
103 Biowest) (complete medium) for 7 days in the presence of 1000 U/ml GM-CSF or 10 ng/ml M-CSF
104 (ImmunoTools) to generate GM-CSF-polarized macrophages (GM-MØ) or M-CSF-polarized
105 macrophages (M-MØ), respectively [27]. Cytokines were added every two days and cells were
106 maintained at 37°C in a humidified atmosphere with 5% CO_2 and 21% O_2. Alveolar macrophages
107 (AMØ) were obtained from remains of bronchoalveolar lavage (BAL) of patients undergoing
108 bronchoscopy for diagnostic purposes under a protocol approved by the Internal Review Board of
109 Instituto de Investigación Hospital 12 de Octubre (Reference TP24/0183). BAL procedure was
110 performed with a flexible bronchoscope and a total volume of 150 ml of sterile isotonic saline
111 solution at 37°C. BAL fluid fractions were maintained at 4°C and cellular debris removed using a 40
112 µm cell strainer. BAL cells were washed with PBS, centrifuged and resuspended in complete
113 medium containing 100 U/mL penicillin and 100 µg/mL streptomycin (#15140-122,Gibco), 50
114 µg/ml gentamicin (#G1397, Sigma-Aldrich), and 2.5 µg/ml amphotericin B (#A2942, Sigma-Aldrich).
115 The cells were seeded at 6–8 × 10^5 cells per well in 12-well plates for 1 h and washed extensively
116 to remove non-adherent cells. Finally, 2 ml of complete medium with antibiotics was added to
117 each well and the adherent cells incubated for 16–18 h before treatments. More than 95% of
118 adherent BAL cells were identified as AMØ according to morphology and phenotypic analysis.
119 When indicated, monocytes, GM-MØ or AMØ were exposed to the GSK3 inhibitors CHIR99021 (10

120 μM), SB-216763 (10 μM) or LiCl (10 mM), using DMSO as control. For macrophage activation, cells
121 were treated with either 100 ng/ml CL264 (InvivoGen), 10 ng/ml *E. coli* 0111:B4 lipopolysaccharide
122 (LPS-EB Ultrapure, Invivogen), TNF (20 ng/ml, ImmunoTools) or IFNγ (5 ng/ml, ImmunoTools).
123 Human cytokine production was measured in M-MØ culture supernatants using commercial ELISA
124 [CCL2 (BD Biosciences), IL-10, CCL18, LGMN, SPP1 (R&D Systems) and activin A (BD Biosciences)]
125 and following the procedures supplied by the manufacturers.

126 **siRNA transfection**. GM-MØ (1×10^6 cells) were transfected with a human *GSK3A*-specific and/or
127 *GSK3B*-specific siRNA (50 nM) (Dharmacon) using HiPerFect (Qiagen). Silencer Select Negative
128 Control No. 2 siRNA (siCtrl, 50 nM) (Dharmacon) was used as negative control siRNA. Six hours
129 after transfection, cells were either allowed to recover from transfection in complete medium (66
130 hours), and lysed. Knockdown of GSK3α/β was confirmed by Western blot.

131 **Quantitative real-time RT-PCR (qRT-PCR)**. Total RNA was extracted using the total RNA and
132 protein isolation kit (Macherey-Nagel). RNA samples were reverse-transcribed with High-Capacity
133 cDNA Reverse Transcription reagents kit (Applied Biosystems) according to the manufacturer's
134 protocol. Real-time quantitative PCR was performed with LightCycler® 480 Probes Master (Roche
135 Life Sciences) and Taqman probes on a standard plate in a Light Cycler® 480 instrument (Roche
136 Diagnostics). Gene-specific oligonucleotides (*IL10*: Forward, 5´-TCACTCATGGCTTTGTAGATGC-3´,
137 and Reverse, 5´- GTGGAGCAGGTGAAGAATGC-3´; *LGMN*: Forward, 5´-
138 GAACACCAATGATCTGGAGGA-3´, and Reverse, 5´-GGAGACGATCTTACGCACTGA-3´) were designed
139 using the Universal ProbeLibrary software (Roche Life Sciences). Results were normalized to the
140 expression level of the endogenous references genes (*TBP*, *HPRT1*) and quantified using the ΔΔCT
141 (cycle threshold) method.

142 **Western blot**. Cell lysates were subjected to SDS-PAGE (50 μg unless indicated otherwise) and
143 transferred onto an Immobilon-P polyvinylidene difluoride membrane (PVDF; Millipore). After

144 blocking the unoccupied sites with 5% non-fat milk diluted in Tris-Buffered Saline plus Tween 20
145 (TBS-T), protein detection was carried out with antibodies against MAFB (HPA005653, Sigma
146 Aldrich), total GSK3α (#4337, Cell Signaling Technology), total GSK3β (#27C10, Cell Signaling
147 Technology), total GSK3 (#5676, Cell Signaling Technology), p-Ser^{9}-GSK3β (#5558, Cell Signaling
148 Technology), p-Ser^{21}-GSK3α (#9316, Cell Signaling Technology), p-Tyr^{279}/P-Tyr^{216}- GSK3α/β (#05-
149 413, Sigma Aldrich), CD163 (#MCA1853, Bio-Rad), MAF (sc-518062, Santa Cruz Biotechnology),
150 IL7R (sc-514445, Santa Cruz Biotechnology) and FOLR2 (clone 94b, kindly provided by Dr. Takami
151 Matsuyama) [39], and vinculin (#V9131, Sigma-Aldrich) or GAPDH (sc-32233, Santa Cruz
152 Biotechnology) as protein loading controls. Quimioluminiscence was detected in a Chemidoc
153 Imaging system (BioRad) using SuperSignal™ West Femto (ThermoFisher Scientific).
154 **RNA-sequencing and data analysis**. RNA isolated from GM-MØ exposed to DMSO or the GSK3β
155 inhibitor CHIR-99021 (10 μM) for 48h, monocytes exposed to CHIR99021 or DMSO, *ex vivo* isolated
156 AMØ exposed to CHIR99021 or DMSO, or GM-MØ transfected with siRNA specific for *GSK3A*
157 and/or *GSK3B*, or a control siRNA, were subjected to sequencing on a BGISEQ-500 platform
158 (https://www.bgitechsolutions.com). RNAseq data were deposited in the Gene Expression
159 Omnibus (http://www.ncbi.nlm.nih.gov/geo/) under accession GSE256538 (monocytes exposed to
160 CHIR99021 or DMSO), GSE256208 (GM-MØ exposed to CHIR99021 or DMSO), GSE262463 (AMØ
161 exposed to CHIR99021 or DMSO) or GSE266236 (GM-MØ transfected with siRNA specific for
162 *GSK3A*, *GSK3B* or a control siRNA). Low quality reads and reads with adaptors or unknown bases
163 were filtered to get the clean reads. Sequences were mapped to GRCh38 genome using HISAT2 [40]
164 or Bowtie2 [41], and clean reads for each gene were calculated using htseq-count [42] and the RSEM
165 software package [43]. Differential gene expression was assessed by using the R-package DESeq2.
166 Differentially expressed genes were analysed for annotated gene sets enrichment using ENRICHR

167 (http://amp.pharm.mssm.edu/Enrichr/) [44,45], and enrichment terms considered significant with a
168 Benjamini-Hochberg-adjusted p value <0.05. For gene set enrichment analysis (GSEA)
169 (http://software.broadinstitute.org/gsea/index.jsp) [46], gene sets available at the website, as well
170 as gene sets generated from publicly available transcriptional studies
171 (https://www.ncbi.nlm.nih.gov/gds), were used. The datasets used throughout the manuscript
172 (either reported here for the first time or previously published) are listed and described in Table
173 S1.

174 **Re-analysis of single cell RNA-seq data.** Single cell RNA-Seq data from 8 healthy lung samples
175 were obtained from GSE128033 [47] and futher analyzed using R programming language. A total of
176 5898240 cells were filtered down to 21310 according to the following criteria: 1) number of genes
177 per cell (nFeature, > 200 and < 6000); 2) Unique Molecular Identifiers (nCount, > 1000) ; and 3) %
178 of mitochondrial genes (< 15 %). Data were then normalized using LogNormalize with a scale
179 factor of 10000 and the top 2000 features were identified with the vst method using Seurat
180 v.5.0.1. The resulting Seurat object was converted into an Anndata object using sceasy v.0.0.7 and
181 the integration was processed using scVI v.1.0.4 and Scanpy v.1.9.8 in a Python enviroment. The
182 trained model was re-converted into a Seurat object. The Seurat FindNeighbors function was used
183 with the scVI reduction to obtain the resulting clusters with a resolution of 1.2. To focus on
184 macrophages and monocytes, macrophage (*CD163*, *FABP4*, *LYVE1* as markers) and monocyte
185 (*FCN1* as marker) clusters were identified and re-integrated using scVI v.1.0.4 in a Python
186 enviroment and later re-clustered in Seurat v.5.0.1 with a resolution of 0.6.

187 **Phagocytosis assay.** Phagocytosis ability was assessed by flow cytometry using pHrodo Red *E. coli*
188 BioParticles Conjugates (Thermo Fisher), following the procedures recommended by the
189 manufacturer. Macrophages were cultured in 24-well plate and exposed to pHrodo bioparticles for
190 60 min at 37 °C/5% CO2. Cells were then harvested and assessed by flow cytometry.

191 **Efferocytosis assay.** Jurkat cells were cultured in RPMI 1640 medium without FCS for 16 h, and
192 then treated with staurosporine (0.5 µg/ml, SIGMA), followed by an incubation at 37 °C for 3 h.
193 Staurosporine treatment yielded a population of 83% annexin V+cells. Apoptotic cells (AC) were
194 resuspended at a concentration of 1×10^6 cells/ml and labeled with CellTrace™ Violet reagent
195 (0.5 µM, Invitrogen, Thermo Scientific) for 20 min. For efferocytosis, macrophages were cultured
196 with labeled AC (ratio 1:4) in p24 plates during 1 h at 37 °C. After 1 h, macrophages were rinsed
197 with PBS to remove unbound AC and detached with PBS 5 mM EDTA, and pelleted by
198 centrifugation before analyzing by flow cytometry.

199 **Bioenergetics profile**. The XF24 extracellular flux analyzer (Seahorse Biosciences, North Billerica,
200 MA) was used to determine the bioenergetic profile of intact cells. Briefly, cells were seeded
201 (200,000 cells/well) in XF24 plates (Seahorse Biosciences) and allowed to recover for 24 h. Cells
202 were then incubated in bicarbonate-free DMEM (Sigma-Aldrich) supplemented with 11.11 mM
203 glucose, 2 mM L-glutamine, 1 mM pyruvate, and 2% FBS (Sigma-Aldrich) in a CO2-free incubator
204 for 1 h. The oxygen consumption rate (OCR) and extracellular acidification rate (ECAR), a proxy for
205 lactate production, were recorded to assess the mitochondrial respiratory activity and glycolytic
206 activity, respectively. After four measurements under basal conditions, cells were treated
207 sequentially with 1 µM oligomycin, 0.6 µM carbonyl cyanide p-(trifluoromethoxy)phenylhydrazone
208 (FCCP), 0.4 µM FCCP, and 0.5 µM rotenone plus 0.5 mM antimycin A (Sigma-Aldrich), with three
209 consecutive determinations under each condition that were subsequently averaged.
210 Nonmitochondrial respiration (OCR value after rotenone plus antimycin A addition) was
211 subtracted from all OCR measurements. ATP turnover was estimated from the difference between
212 the basal and the oligomycin-inhibited respiration, and the maximal respiratory capacity was the
213 rate in the presence of the uncoupler FCCP [48]. Six independent replicas of each analysis were done,
214 and results were normalized according to protein concentration.

215 **Multicolor Fluorescence Confocal Microscopy**

216 Lung samples were collected from autopsies performed on patients who died from diagnosed
217 SARS-CoV-2 infection or unrelated causes (myocardial infarction, as controls) at the Gregorio
218 Marañón Hospital, Madrid. Patient data and samples were obtained in accordance with Ethics
219 Committees of Instituto de Investigación Sanitaria Gregorio Marañón requirements. Formalin-
220 fixed and paraffin-embedded tissues were deparaffinized, rehydrated, and unmasked by steaming
221 in 10 mM sodium citrate buffer pH 9.0 (Dako Glostrup, Denmark) for 7 minutes. Slides were
222 blocked with 5 µg/ml human immunoglobulins solved in blocking serum-free medium (Dako) for
223 30 minutes, and then sequentially incubated with 5–10 µg/ml primary antibodies, overnight at
224 4°C, and proper fluorescent secondary antibodies (Jackson Immunoresearch, West Grove, PA, US)
225 for 1h. Washes were performed by immersion in PBS containing 0.05% Tween-20, and single-cell
226 quantification was performed in 3–5 fields imaged with the ACS_APO 20x/NA 0.60 objective of a
227 confocal microscope (Leica, SPE). Mean Fluorescence Intensity (MFI) of proteins of interest was
228 obtained at segmented CD68+ macrophages using the 'analyze particle' plugging of ImageJ2
229 software [49], as previously shown [50].

230 **Statistical analysis**. Statistical analyses were conducted using the GraphPad Prism software. For
231 comparison of means, and unless otherwise indicated, statistical significance of the generated
232 data was evaluated using the paired Student t test or One-Way ANOVA followed by multiple
233 comparisons using the Dunnett's test or Fisher´s LSD test. In all cases, $p<0.05$ was considered as
234 statistically significant.

235

236 **RESULTS**

237 **Monocyte-derived macrophages generated in the presence of GM-CSF (GM-MØ) or M-CSF (M-**
238 **MØ) differ in the state of activation of GSK3α and GSK3β.** Monocyte-derived M-MØ exhibit a
239 transcriptional profile akin to that of pathogenic macrophages in severe COVID-19 [22], whereas GM-
240 MØ resemble lung alveolar macrophages (AMØ) [22]. Our prior research has established that MAFB
241 determines the transcriptional and functional specification of monocyte-derived M-MØ,
242 characterized by significantly higher MAFB levels compared to GM-MØ [27]. Since the protein levels
243 of large MAF family members (MAF, MAFA, MAFB, NRL) are controlled through GSK3
244 phosphorylation-dependent proteasome degradation [30], we initially assessed the relative levels of
245 the inhibitory (Ser^{21} for GSK3α and Ser^{9} for GSK3β) and activation-associated (Tyr^{279} for GSK3α
246 and Tyr^{216} for GSK3β) phosphorylation of GSK3 in M-MØ and GM-MØ. Ser^{21}-GSK3α and Ser^{9}-
247 GSK3β phosphorylation was more pronounced in M-MØ, aligning with their elevated levels of
248 MAFB (Figure 1A). Conversely, no significant difference in Tyr^{279}-GSK3α and Tyr^{216}-GSK3β
249 phosphorylation was observed between M-MØ and GM-MØ (Figure 1B). Therefore, the
250 heightened expression of MAFB in M-MØ correlates with a higher inhibitory phosphorylation of
251 GSK3.

252

253 **Inhibition of GSK3 leads to transcriptional, phenotypic, functional, and metabolic**
254 **reprogramming in monocyte-derived GM-MØ.** Building upon the above findings, we aimed to
255 examine the macrophage re-programming effects of GSK3 activity modulation in GM-MØ through
256 the use of the GSK3 inhibitor CHIR-99021 (Figure 1C). Kinetics and dose-response analysis of the
257 effects of CHIR-99021 on MAFB expression showed that maximal protein levels were achieved
258 after a 24-48 hour exposure to 10μM CHIR-99021 (Supplementary Figure 1A), conditions that were

259 used hereafter. Indeed, treatment of GM-MØ with CHIR-99021 for 48 hours resulted in a
260 significant decrease in the activation-associated Tyr^{216}-GSK3β phosphorylation (Figure 1D) and a
261 robust elevation in MAFB protein levels (Figure 1E). Moreover, reversal of the Tyr^{216}/Ser^{9} GSK3β
262 phosphorylation ratio was also seen after CHIR-99021 treatment, albeit it was not observed after
263 exposure to other GSK3 inhibitors (SB-216763 or LiCl; Supplementary Figure 1B). RNA-Seq analysis
264 of CHIR-GM-MØ unveiled a huge transcriptional impact of GSK3 inhibition, with more than 2000
265 differentially expressed genes ([$\log_2$FC]>1; *adj p* < 0.05) (Figure 1F). Corresponding with the higher
266 MAFB expression, Gene Set Enrichment Analysis (GSEA) showed that the CHIR-GM-MØ
267 transcriptome was significantly enriched in genes that either mark M-MØ (GSE68061) or are
268 upregulated during monocyte-to-M-MØ differentiation (Figure 1G). Conversely, GM-MØ-specific
269 genes (GSE68061) or genes increased during monocyte-to-GM-MØ differentiation, were
270 downregulated (Figure 1G). Additional gene ontology analysis further supported the
271 pathophysiological significance of the macrophage re-programming induced by modulating GSK3
272 activity. Thus, analysis of the MoMac-VERSE (a resource that identified conserved monocyte and
273 macrophage states derived from healthy and pathologic human tissues) (GSE178209) [2], indicated
274 that GSK3 inhibition augments the expression of the gene sets that define MoMac-VERSE subsets
275 identified as long-term resident macrophages [Cluster HES1_Mac (#2)] and tumor-associated
276 macrophages with an M2-like signature [Clusters HES1_Mac (#2), TREM2_Mac (#3), $C1Q^{hi}$_Mac
277 (#16) and FTL_Mac (#17)] [2] (Figure 1H). Moreover, GSK3 inhibition increased the expression of the
278 gene sets that define pathogenic pro-fibrotic macrophage subsets in severe COVID-19 [(Group 3 or
279 $SPP1^{+}$, GSE145926) [24], MoAM3 (GSE155249) [25] or $CD163^{+}/LGMN^{+}$ MØ (EGAS00001005634) [23]]
280 (Figure 1I). Therefore, GSK3 inhibition enhances MAFB expression and re-programs macrophage
281 by promoting the acquisition of the gene profile that defines anti-inflammatory and pro-fibrotic
282 macrophages.

283

284 In agreement with the increased MAFB levels detected in CHIR-GM-MØ (Figure 1E), screening for
285 mediators of the re-programming action of GSK3 inhibition using DoRoThEA [51]
286 (https://saezlab.github.io/dorothea/) revealed a significant enrichment in MAFB-regulated genes
287 (Figure 2A), and similar results were yielded upon Enrichr analysis
288 [44,45](https://maayanlab.cloud/Enrichr/) (Supplementary Figure 1C). In fact, GSEA confirmed that
289 CHIR-GM-MØ are enriched in MAFB-dependent genes [22,27] (Figure 2B-C) along with macrophage
290 genes whose regulatory regions are directly bound by MAFB [52] (75-geneset, Figure 2C), including
291 *CCL2*, *CCL8*, *CCL18*, *IGF1*, *IL10* and *LGMN* (Figure 2D). Importantly, all these changes were reflected
292 in the phenotype of CHIR-GM-MØ, that showed elevated expression of transcription factors like
293 MAF (Figure 2E), cell surface proteins like CD163 and FOLR2 (Figure 2E, F), and soluble factors like
294 CCL2, CCL18, IL-10, LGMN and SPP1 (Figure 2G), all of which are either direct MAFB targets [52] or
295 MAFB-regulated genes [22,27]. Likewise, the attenuated expression of the GM-MØ-specific *INHBA*
296 gene (Figure 2D) corresponded to a decrease in Activin A production by CHIR-GM-MØ (Figure 2G).
297 These results underscore the phenotypic re-programming induced by GSK3 inhibition in GM-MØ,
298 wherein there is an upregulation of MAFB-dependent transcription factors, cell surface markers,
299 and soluble factors which collectively define an anti-inflammatory/pro-fibrotic phenotype
300 characteristic of M-CSF-dependent monocyte-derived macrophages.

301

302 Remarkably, the phenotypic changes induced by GSK3 inhibition were also accompanied by
303 alterations in macrophage functional capabilities. Thus, CHIR-GM-MØ exhibited elevated anti-
304 inflammatory activity, evidenced by increased production of IL-10 upon activation by
305 inflammatory cytokines such as TNF or IFNγ, or exposure to PAMPs like LPS or the TLR7 ligand
306 CL264 (Figure 3A). In addition, CHIR-GM-MØ demonstrated increased phagocytic ability for *E. coli*

307 particles (Figure 3B), as well as enhanced efferocytosis (Figure 3C), with both activities being
308 typically higher in M-MØ. Collectively, these findings indicate that GSK3 inhibition re-educates
309 GM-MØ macrophages by facilitating the acquisition of transcriptional, phenotypic, and functional
310 properties characteristic of M-CSF-dependent monocyte-derived macrophages. Of note, in line
311 with the well-established connection between inflammatory potential and metabolic state in
312 macrophages [53], GSK3 inhibition also induced modifications in various metabolic parameters in
313 GM-MØ, including basal respiration and maximal ATP production (Supplementary Figure 1D-F).
314
315 **siRNA-mediated knock-down of *GSK3A* and/or *GSK3B* enhances the expression of the MAFB-**
316 **dependent profiles of M-MØ and pathogenic pro-fibrotic lung macrophages.** To fully support the
317 involvement of GSK3 in the macrophage re-programming action of CHIR-99021, we next assessed
318 the transcriptional consequences of knocking-down *GSK3A* (coding for GSK3α) and/or *GSK3B*
319 (coding for GSK3β) in GM-MØ (Figure 4A,B). Like CHIR-99021, silencing of both *GSK3A* and *GSK3B*
320 augmented the expression of MAFB, with the simultaneous silencing of both *GSK3A* and *GSK3B*
321 genes having a stronger effect (Figure 4B), and modulated the expression of 329 genes (Figure
322 4C,D). Of note, silencing of *GSK3A* and *GSK3B* reproduced the effects of CHIR-99021, as it strongly
323 enhanced the expression of genes upregulated by the inhibitor in either GM-MØ or *ex vivo*
324 isolated Alveolar Macrophages (Figure 4E and not shown). *GSK3A/B* knock-down triggered a
325 significant enrichment in the expression of MAFB-dependent genes (Figure 4F), genes acquired
326 along the monocyte-to-M-MØ differentiation (Figure 4G), and genes that mark M-MØ, while
327 reducing the expression of GM-MØ-specific genes (Figure 4G). Furthermore, in agreement with
328 the effect of CHIR-99021, *GSK3A/B* knock-down enhanced the expression of the MoMac-VERSE
329 macrophage clusters HES1_Mac (#2) and TREM2_Mac (#3) [2] (Figure 4H) as well as the gene sets
330 that define pathogenic pro-fibrotic macrophage subsets in severe COVID-19 [(SPP1^{+}, GSE145926)

331 [24], MoAM3 (GSE155249) [25] or CD163$^+$/LGMN$^+$ MØ (EGAS00001005634) [23]] (Figure 4I,
332 Supplementary Figure 2A). Conversely, silencing of *GSK3A* and *GSK3B* drastically reduced the
333 expression of the gene sets that characterize tissue-resident lung Alveolar Macrophages in COVID-
334 19, with the concomitant silencing of *GSK3A* and *GSK3B* again showing a stronger effect (Figure
335 4I). Altogether, these results support the relevance of GSK3α and GSK3β as relevant targets for
336 human macrophage re-programming.
337
338 **GSK3 inhibition redirects monocytes towards acquiring a gene profile reminiscent of anti-**
339 **inflammatory M-MØ.** Given the swift and profound anti-inflammatory impact observed in fully
340 differentiated GM-MØ upon GSK3 inhibition or knock-down, we next delved into assessing
341 whether modulation of GSK3 activity influence the differentiation capability of peripheral blood
342 monocytes. To that end, monocytes were exposed to CHIR-99021, and the resulting cells (CHIR-
343 Mon, Figure 5A) exhibited increased MAFB levels as early as 16 hours post-treatment (Figure 5B).
344 Remarkably, the 16-hour exposure to the GSK3 inhibitor induced significant alterations in the
345 expression of over 2000 genes ([$\log_2$FC]>1; *adj p* < 0.05) (Figure 5C) and sufficed to augment the
346 expression of M-MØ-specific genes and genes upregulated during M-CSF-dependent monocyte-to-
347 M-MØ differentiation (Figure 5D), including *CCL2*, *CD163* and *IL10* (Figure 5E). Notably, the
348 transcriptome of CHIR-Mon exhibited a significant enrichment in MAFB-dependent genes (Figure
349 5F, Supplementary Figure 2B) and genes characterizing the MAFB+ pathogenic macrophages in
350 severe COVID-19 (Supplementary Figure 2C), whereas it showed an under-representation of genes
351 inhibited by MAFB [52] (Figure 5F). Compared to DMSO, CHIR-99021 treatment upregulated the
352 expression of 25% of M-MØ-specific genes, including MAFB-dependent genes like *CCL2*, *IL10* and
353 *CD163*, while downregulating 30% of GM-MØ-specific genes (Figure 5G), and this transcriptional
354 effect was also evident in comparison with M-CSF-treated monocytes (Supplementary Figure 2D).

355 To broaden the scope of these findings, we also examined the consequences of inhibiting GSK3 in
356 monocytes exposed to a pathologic pro-inflammatory environment, namely synovial fluid from
357 patients with active rheumatoid arthritis (RASF) (Figure 5H). Evaluation of CHIR-99021-treated
358 monocytes in the presence of RASF revealed an enhanced expression of MAFB (Figure 5I) and
359 MAFB-dependent genes such as *IL10* and *LGMN* (Figure 5J). Therefore, GSK3 inhibition in
360 monocytes also leads to heightened MAFB expression, ultimately steering differentiation towards
361 anti-inflammatory monocyte-derived macrophages.
362
363 **Inhibition of GSK3 in *ex vivo* isolated human alveolar macrophages promotes the acquisition of**
364 **an M-MØ-like anti-inflammatory profile.** To further validate the macrophage re-programming
365 potential of GSK3 inhibition, we next conducted experiments on *ex vivo* isolated human alveolar
366 macrophages (AMØ, Figure 6A), whose development and gene expression profile is GM-CSF-
367 dependent [17–19]. To that end, we determined the transcriptome of three independent isolates of
368 AMØ, purified from broncho-alveolar lavages, after exposure to CHIR-99021 for 24 hours (Figure
369 6A). A total of 865 differentially expressed genes ([$\log_2$FC]>1; *adj p* < 0.05) were identified, with
370 316 genes upregulated in CHIR-AMØ (Figure 6B). Further comparisons and gene ontology analysis
371 revealed that GSK3 inhibition by CHIR-99021 (CHIR-AMØ) upregulated the gene sets that define
372 pathogenic pro-fibrotic macrophage subsets in severe COVID-19 [(SPP1$^+$, GSE145926) [24], MoAM3
373 (GSE155249) [25] or CD163$^+$/LGMN$^+$ MØ (EGAS00001005634) [23]] (Figure 6C,D; Supplementary Figure
374 2E). Conversely, CHIR-AMØ exhibited a reduced expression of the gene sets that characterize lung-
375 resident AMØ in severe COVID-19 [AMØ1+AMØ2 clusters from EGAS00001005634) [23], FABP4+
376 from GSE145926) [24], TRAM1 from GSE155249 [25]] (Figure 6D,E; Supplementary Figure 2F), including
377 key AMØ-specific genes like *FABP4* and *MARCO* (Figure 6E), and similar resuts were seen upon
378 analysis of AMØ-specific gene sets from other studies [25,54] (Supplementary Figure 2F). Like in the

379 case of CHIR-GM-MØ, CHIR-AMØ exhibited an over-representation of M-MØ-specific genes and
380 genes acquired along the monocyte-to-M-MØ differentiation (GSE188278) (Supplementary Figure
381 2G). Consistent with these findings, CHIR-AMØ exhibited higher expression of MAFB (Figure 6F)
382 whose increase correlated with an augmented secretion of Legumain, CCL2 and IL-10 (Figure 6G),
383 although the latter was only seen in two samples, probably reflecting heterogeneity in primary cell
384 responses. In contrast, lower levels of activin A were detected in CHIR-AMØ-conditioned medium
385 (Figure 6G). Remarkably, and in agreement with the shift in macrophage subsets that takes place
386 in severe COVID-19 lungs (loss of AMØ, appearance of monocyte-derived pro-fibrotic
387 macrophages) [22–25], the level of phosphorylated Ser^{21}-GSK3α and Ser^{9}-GSK3β was very significantly
388 augmented in lung macrophages (CD68+) from severe COVID-19 patients, an increase that
389 correlated with a robust enhancement of the macrophage expression of both MAFB and the
390 MAFB-dependent protein CD163 (Figure 6H). These results collectively demonstrate that
391 macrophage re-programming through GSK3 inhibition can also be achieved on *in vivo* isolated
392 macrophages, leading to enhanced expression of MAFB and MAFB-dependent genes, the
393 acquisition of an anti-inflammatory transcriptional profile and the loss of the signature of lung-
394 resident human AMØ.
395
396 **GSK3- and MAFB-dependent genes are differentially expressed between human lung alveolar**
397 **and interstitial macrophages.** To assess whether GSK3 inhibition also modulates the phenotypic
398 differences between human lung macrophage subsets in a physiological setting, we next took
399 advantage of the available information on human healthy lungs obtained by single cell-RNA
400 sequencing [47]. Re-analysis of the single cell-RNA sequencing data [47] (Figure 7A; Supplementary
401 Figure 3A-D) revealed several clusters expressing macrophage-associated markers (*CD163*, *FABP4*,
402 *LYVE1, FCN1*) (Supplementary Figure 3D), and whose subsequent re-clustering identified cell

403 subsets expressing previously defined markers for infiltrating monocytes (Cluster 4/7/12:*FCN1*) [23],
404 Alveolar macrophages (AMØ) (Clusters 0/2/5/13: *FABP4 TYMS*-negative; Cluster 9: *MARCO*,
405 *INHBA; Cluster 11: PPARG*), proliferating AMØ (Cluster 15: *TYMS, MKI67, TOP2A, NUSAP1*) [23], and
406 Interstitial Macrophages (IMØ) that variably express markers for tissue-resident macrophages like
407 *LYVE1, RNASE1* and *LGMN* (Clusters 1/3/6/8/10/14) [1,23,47] (Figure 7B; Supplementary Figure 4A-C).
408 The comparison of IMØ and AMØ subsets revealed that the genes upregulated upon inhibition of
409 GSK3 include numerous MAFB-dependent genes (e.g., *MAFB*, *IL10*, *LGMN*, *SPP1*, *CCL2*) and
410 showed a higher expression in IMØ (Figure 7C). On the other hand, the genes downregulated by
411 CHIR-99021 were preferentially or exclusively expressed in AMØ, including *INHBA*, *GSN*, *FBP1*,
412 *PPARG*, *AXL* and *AQP3* (Figure 7C). Therefore, GSK3 inhibition prompts macrophages towards the
413 acquisition of a gene profile that resembles that of IMØ, while provokes the loss of the AMØ gene
414 signature. Such a conclusion was also reached upon analysis of pseudo bulk-RNA sequencing data
415 from GSE128033 [47]. Indeed, numerous MAFB-dependent and GSK3-regulated genes were found
416 within the 712 genes that are differentially expressed ([$\log_2$FC]>1; *adj p* < 0.05) between IMØ and
417 AMØ (Figure 7D). Further GSEA evidenced that GSK3 inhibition in either GM-MØ (CHIR-GM-MØ)
418 (Figure 7E) or AMØ (CHIR-AMØ) (Figure 7F) very significantly enhance the expression of MAFB-
419 dependent IMØ-specific genes (as defined by Morse *et al.* [47] or by Li *et al.* [55]), while simultaneosuly
420 impaired the expression of genes characterizing human AMØ (Figure 7E-F). More importantly, a
421 similar effect was observed after *GSK3A/B* silencing in GM-MØ, that yielded an enhanced
422 expression of IMØ-specific genes and a downregulation of the gene set that defines AMØ (Figure
423 7G). Altogether, these results indicate that inhibiting GSK3 shifts the gene profile of Alveolar
424 Macrophages towards that of Interstitial Macrophages (or monocyte-derived macrophages), and
425 imply that the activation status of GSK3 significantly influences the specification of lung-resident
426 macrophages (AMØ *vs*. IMØ).

427 **DISCUSSION**

428 Our previous investigations have demonstrated that the macrophage re-programming effect of
429 LXR modulators [38,56] and methotrexate [37] coincide with alterations in the protein levels of MAFB.
430 Similarly, intravenous immunoglobulins have been shown to alter the inflammatory state of
431 macrophages and modulate MAFB levels [57]. Building upon these findings and others, we have
432 explored whether modulating the activity of GSK3, a primary regulator of MAFB protein levels and
433 activity, is sufficient to induce a shift in the inflammatory profile of human macrophages. Our
434 results indicate that GSK3 inhibition impairs the expression of genes associated with GM-CSF-
435 dependent differentiation of monocyte-derived macrophages while concurrently promoting the
436 acquisition of genes and functions associated with M-CSF-dependent monocyte-derived
437 macrophages, particularly those regulated by MAFB. The physiological relevance of these findings
438 is underscored by the contrasting effect that GSK3 inhibition has on genes that define lung-
439 resident alveolar macrophages (decrease) versus monocyte-derived macrophages recruited into
440 the lung (increase) during inflammatory responses. Thus, modulation of GSK3 activity emerges as a
441 plausible strategy for macrophage reprogramming in therapeutic interventions.

442

443 Therapeutic approaches aimed at re-educating tumor-associated macrophages into
444 immunostimulatory cells [58] may involve targeting the macrophage PI3Kγ intracellular signaling
445 pathway [59], which inhibits NFκB activation through Akt and mTOR [60], thereby inducing an anti-
446 inflammatory program that promotes immune suppression. Indeed, macrophage PI3Kγ
447 inactivation stimulates and prolongs NFκB activation, promoting an immunostimulatory
448 transcriptional program [60]. The ability of PI3Kγ to toggle between immune stimulation and
449 suppression aligns with our findings on GSK3 inhibition, as PI3Kγ inactivates GSK3 via
450 phosphorylation of Ser^{9} (GSK3β) and Ser^{21} (GSK3α) [30]. Threfore, GSK3 inhibition may contribute to

451 the anti-inflammatory and immunosuppressive effects of PI3Kγ inactivation by enhancing MAFB
452 expression. Moreover, MAFB might even participate in the macrophage reprogramming
453 consequences of mTOR modulation [61–63] due to the known reciprocal interactions between GSK3
454 and mTOR [64]. Hence, since the phosporylation of MAFB by GSK3 requires of a prior "priming"
455 phosphorylation event [30], identification of the MAFB priming kinase(s) emerges as a potentially
456 relevant effort in the search for additional targets for macrophage re-programming.
457
458 The significant impact of GSK3 inhibition by CHIR-99021 on the macrophage transcriptional profile
459 mirrors the effects observed with other GSK3 inhibitors on the differentiation of monocyte-
460 derived dendritic cells (MDDC) [65]. Specifically, GSK3 inhibitors like LiCl, SB415286, or SB216763
461 redirect the GM-CSF+IL-4-dependent development of MDDC towards the generation of
462 macrophage-like cells [65]. Considering that MAFB expression is higher in monocyte-derived
463 macrophages than in dendritic cells [66], it is reasonable to infer that GSK3 inhibitors also boost
464 MAFB expression in cells differentiated in the presence of GM-CSF+IL-4, thereby supporting the
465 modulation of GSK3 activity as a tool to alter lineage determination in myeloid cells.
466
467 The re-programming effect of GSK3 inhibition on *ex vivo* isolated alveolar macrophages bears
468 significant therapeutic implications, particularly in severe COVID-19 cases where profibrotic
469 monocyte-derived macrophages replace GM-CSF-dependent tissue-resident alveolar macrophages
470 [23,24,67]. Our observations reveal that exposure of *ex vivo* isolated alveolar macrophages to CHIR-
471 99021 leads to the loss of the alveolar macrophage GM-CSF-dependent gene profile and the
472 acquisition of a MAFB-dependent pro-fibrotic transcriptional landscape resembling that of M-CSF-
473 dependent monocyte-derived macrophages. Given that MAFB serves as a negative regulator of
474 GM-CSF signaling [68], downregulation of MAFB expression through modulation of GSK3 activity

475 emerges as a rationale strategy to re-direct pathogenic monocyte-derived macrophages towards
476 the acquisition of a lung-resident alveolar macrophage-like profile during severe COVID-19. This
477 approach aligns with the proposed therapeutic use of GM-CSF in COVID-19 [69,70], as GM-CSF would
478 impede or limit the MAFB-dependent upregulation of profibrotic and neutrophil-attracting factors
479 observed in severe COVID-19 [52].

ACKNOWLEDGEMENTS

This work was supported by grant PID2020-114323RB-I00 from Ministerio de Ciencia e Innovación to ALC, Dirección General de Innovación e Investigación Tecnológica de la Comunidad de Madrid (RETARACOVID, P2022/BMD-7274) to ALC, APK, PS-M and RD, Instituto de Salud Carlos III (Grant PI23/00224 to APK, Grant PI21/00989 to RD), Red de Enfermedades Inflamatorias (RICORS RD21/0002/0034) from Instituto de Salud Carlos III and cofinanced by the European Regional Development Fund "A way to achieve Europe" (ERDF) and PRTR to APK, and PID2021-123167OB-I00 from Ministerio de Ciencia, Innovación y Universidades and CSIC Talent Attraction program (20222AT010) to EO. This research work was also funded by the European Commission – NextGenerationEU (Regulation EU 2020/2094), through CSIC's Global Health Platform (PTI Salud Global). AN-V was funded by YEI program contract from Comunidad de Madrid (PEJ-2021-AI/BMD-23327). IR was funded by a Formación de Personal Investigador predoctoral fellowship from Ministerio de Ciencia e Innovación (Grant PRE2021-097080). Figures were created with Biorender.com.

AUTHORSHIP CONTRIBUTIONS

IR, CH, MT-T, BL-N, MT-S, FD-C, AN-V, RS and YS-P performed research and analyzed data; EO, PS-M, RD, AP-K and ALC designed research and analyzed data; FR-S and RG-L identified suitable patients for broncho-alveolar lavage; IR, APK and ALC wrote the paper.

DISCLOSURE OF CONFLICTS OF INTEREST

The authors declare no competing financial interests.

504 **AVAILABILITY OF DATA AND MATERIALS**

505 The dataset supporting the conclusions of this article is available in the Gene Expression Omnibus
506 repository (http://www.ncbi.nlm.nih.gov/geo/) under accession GSE256538 (monocytes exposed
507 to CHIR99021 or DMSO), GSE256208 (GM-MØ exposed to CHIR99021 or DMSO), GSE262463
508 (alveolar macrophages exposed to CHIR99021 or DMSO) and GSE266236 (GM-MØ after GSK3α/β
509 knockdown).

510 **FIGURE LEGENDS**

511 **Figure 1. Transcriptional effect of GSK3 inhibition on monocyte-derived GM-MØ. A**. MAFB, total
512 GSK3α, total GSK3β, Ser^{9}-phosphorylated GSK3β and Ser^{21}-phosphorylated GSK3α levels in M-MØ
513 and GM-MØ, as determined by Western blot (left panel). GAPDH protein levels were determined
514 as protein loading control. Mean ± SEM of the MAFB/GAPDH, Ser^{21}-phosphorylated GSK3α/total
515 GSK3α and Ser^{9}-phosphorylated GSK3β/total GSK3β protein ratios from three independent
516 experiments are shown (right panel) (paired Student's t test: ***, $p<0.005$; ****, $p<0.001$). A
517 representative Western blot experiment is shown in each case in the upper panel. **B**. p-Tyr^{279}-
518 GSK3α and p-Tyr^{216}-GSK3β levels in four independent samples of M-MØ and GM-MØ, as
519 determined by Western blot (left panel). GAPDH protein levels were determined as protein
520 loading control. Mean ± SEM of the p-Tyr^{279}-GSK3α/GAPDH and p-Tyr^{216}-GSK3β/GAPDH protein
521 ratios from four independent experiments are shown (right panel) (paired Student's t test: n.s.,
522 not significant). **C.** Schematic representation of the exposure of GM-MØ to CHIR-99021 for 48
523 hours. **D.** Tyr^{279}-phosphorylated GSK3α and Tyr^{216}-phosphorylated GSK3β levels in three
524 independent preparations of DMSO- or CHIR-99021-treated GM-MØ, as determined by Western
525 blot (left panel). GAPDH protein levels were determined as protein loading control. Mean ± SEM of
526 the p-Tyr^{216}-GSK3β/GAPDH and p-Tyr^{279}-GSK3α/GAPDH protein ratios from the three independent
527 experiments are shown (right panel) (paired Student's t test: ****, $p<0.001$). **E**. MAFB protein
528 levels in DMSO-GM-MØ and CHIR-GM-MØ, as determined by Western blot. A representative
529 experiment is shown. **F**. Number of differentially expressed genes ([log2FC] >1; adjp<0.05)
530 between DMSO-GM-MØ and CHIR-GM-MØ. Differential gene expression was assessed using
531 DESeq2. **G**. GSEA of the indicated gene sets (from GSE68061, left panel; from GSE188278, right
532 panel) on the ranked comparison of the CHIR-GM-MØ vs. DMSO-GM-MØ transcriptomes.

533 Normalized Enrichment Score (NES) and FDRq values are indicated in each case. **H**. Summary of
534 GSEA of the gene sets that define the tissue-resident monocyte and macrophage states (MoMac-
535 VERSE) [2] on the ranked comparison of the CHIR-GM-MØ vs. DMSO-GM-MØ transcriptomes. FDRq
536 values are indicated only if FDRq>0.0; empty dots, Not Significant. **I.** Summary of GSEA of the gene
537 sets that characterize the macrophage subsets identified in severe COVID-19 [23–25] on the ranked
538 comparison of the CHIR-GM-MØ vs. DMSO-GM-MØ transcriptomes. FDRq values are indicated
539 only if FDRq>0.0; empty dots, Not Significant.

540

541 **Figure 2.- Phenotypic effects of GSK3 inhibition on monocyte-derived GM-MØ: Enhanced**
542 **expression of MAFB-dependent genes and proteins. A.** DoRoThEA [51] analysis on the ranked
543 comparison of the DMSO-GM-MØ and CHIR-GM-MØ transcriptomes. **B**. GSEA of MAFB-regulated
544 gene sets (from GSE155719) on the ranked comparison of the DMSO-GM-MØ and CHIR-GM-MØ
545 transcriptomes. NES and FDRq values are indicated in each case **C**. Overlap between the genes
546 upregulated (|log2FC|>1; adjp<0.05) in CHIR-GM-MØ (relative to DMSO M-MØ) and MAFB-
547 dependent genes (from GSE155719, left panel) or the 75-geneset of MAFB-regulated genes (right
548 panel) [52], with indication of some of the overlapping genes. **D**. Relative mRNA levels of the
549 indicated genes in DMSO-GM-MØ and CHIR-GM-MØ, as determined by RNA-Seq on three
550 independent samples (GSE256208). *Adjp* of the comparison, shown in each case, was assessed
551 using DESeq2. **E**. CD163, MAF and IL7R protein levels in DMSO-GM-MØ and CHIR-GM-MØ, as
552 determined by Western blot (left panel). GAPDH protein levels were determined as protein
553 loading control. Mean ± SEM of the MAF/GAPDH, IL7R/GAPDH and CD163/GAPDH protein ratios
554 from seven independent experiments are shown (right panels) (paired Student's t test: ***,
555 p<0.005; ****, p<0.001). A representative Western blot experiment is shown in each case. **F**.
556 FOLR2 protein levels in DMSO-GM-MØ and CHIR-GM-MØ, as determined by Western blot (left

557 panel). Vinculin protein levels were determined as protein loading control. Mean ± SEM of the
558 FOLR2/Vinculin protein ratio from three independent experiments are shown (lower panel)
559 (paired Student's t test: **, p<0.01). A representative Western blot experiment is shown. **G**.
560 Production of the indicated soluble factors by DMSO-GM-MØ and CHIR-GM-MØ, as determined by
561 ELISA. Mean ± SEM of seven independent samples are shown (paired Student's t test: *, p<0.05;
562 **, p<0.01; ***, p<0.005; ****, p<0.001).
563
564 **Figure 3.- Functional consequences of GSK3 inhibition on monocyte-derived GM-MØ. A.**
565 Production of IL-10 by untreated (-) or stimulated (LPS, TNF, IFNγ or CL264) DMSO-GM-MØ and
566 CHIR-GM-MØ, as determined by ELISA. Mean ± SEM of four independent samples are shown
567 (paired Student's t test: *, p<0.05; **, p<0.01; ***, p<0.005; ****, p<0.001). **B.** Phagocytosis of
568 pHRodo-labeled bacterial particles by DMSO-GM-MØ and CHIR-GM-MØ, as determined by flow
569 cytometry. Mean ± SEM of three independent samples are shown (paired Student's t test: *,
570 p<0.05). A representative flow cytometry analysis is shown in the left panel. **C**. Efferocytosis
571 capacity of DMSO-GM-MØ, CHIR-GM-MØ and DMSO-M-MØ, as determined by flow cytometry
572 using staurosporine-induced CellTrace Violet-labeled apoptotic Jurkat cells. The percentage of
573 positive cells and mean fluorescence intensity are shown. Mean±SEM of 3 independent samples
574 are shown (one-way ANOVA with Fisher LSD test: *, p<0.05; **, p<0.01; ***, p<0.005).
575 Representative flow cytometry histograms for CellTrace Violet emission of DMSO-GM-MØ, CHIR-
576 GM-MØ and DMSO-M-MØ are shown.
577
578 **Figure 4.- Transcriptional effects of GSK3 knock-down in monocyte-derived GM-MØ. A.**
579 Schematic representation of the siRNA-mediated GSK3 knock-down procedure in monocyte-
580 derived GM-MØ. **B**. Total GSK3α, GSK3β and MAFB protein levels in monocyte-derived GM-MØ

581 after siRNA-mediated *GSK3A* and/or *GSK3B* silencing, as determined by Western blot (upper
582 panel). GAPDH protein levels were determined as protein loading control. Mean ± SEM of
583 GSK3β/GAPDH and GSK3α/GAPDH protein ratios from the three independent experiments are
584 shown (lower panel) (one-way ANOVA with Dunnet test:*, p<0.05). **C**. Heatmap of the relative
585 expression of the genes significantly altered after *GSK3A* and *GSK3B* knock-down in siCNT-GM-MØ
586 (lanes A-C), siGSK3A-GM-MØ (lanes D-F), siGSK3B-GM-MØ (lanes G-I), siGSK3A/B-GM-MØ (lanes J-
587 L). Representative genes are indicated. **D**. Number of differentially expressed genes (adjp<0.05)
588 between siGSK3A-GM-MØ, siGSK3B-GM-MØ or siGSK3A/B-GM-MØ and siCNT-GM-MØ.
589 Differential gene expression was assessed using DESeq2. **E**. GSEA of the genes whose expression is
590 significantly modulated by CHIR-99021 in either GM-MØ (from Figure 1, this manuscript) or in *ex*
591 *vivo* isolated Alveolar Macrophages (AMØ, see below in Figure 6) on the ranked comparison of the
592 siGSK3A/B-GM-MØ vs. siCNT-GM-MØ transcriptomes. **F.** GSEA of the indicated gene sets (from
593 GSE68061) on the ranked comparison of the siGSK3A/B-GM-MØ vs. siCNT-GM-MØ transcriptomes.
594 **G**. Summary of GSEA of the indicated gene sets (from GSE188278) on the ranked comparison of
595 siGSK3A/B-GM-MØ vs. siCNT-GM-MØ. **H.** Summary of GSEA of the gene sets that define the
596 tissue-resident monocyte and macrophage states (MoMac-VERSE) [2] on the ranked comparison of
597 the siGSK3A/B-GM-MØ vs. siCNT-GM-MØ transcriptomes. FDRq values are indicated only if
598 FDRq>0.0; empty dots, Not Significant. **I.** Summary of GSEA of the gene sets that characterize the
599 macrophage subsets identified in severe COVID-19 [23–25] on the ranked comparison of siGSK3A/B-
600 GM-MØ vs. siCNT-GM-MØ. FDRq values are indicated only if FDRq>0.0; empty dots, Not
601 Significant.

602

603 **Figure 5.- Transcriptional effects of GSK3 inhibition on human peripheral blood monocytes. A.**
604 Schematic representation of the exposure of human monocytes to CHIR-99021 or DMSO for 16h.

605 **B**. MAFB protein levels in monocytes exposed for 16h to DMSO, CHIR-99021 or M-CSF, as
606 determined by Western blot (left panel). Vinculin protein levels were determined as protein
607 loading control. Mean ± SEM of the MAFB/Vinculin protein ratio from the three independent
608 experiments shown (right panel) (one-way ANOVA with Fisher LSD test: ***, p<0.005). **C**. Number
609 of differentially expressed genes ([log2FC] >1; adjp<0.05) between DMSO-Mon and CHIR-Mon.
610 Differential gene expression was assessed using DESeq2. **D**. GSEA of the indicated gene sets (from
611 GSE68061, upper panel; from GSE188278, lower panel) on the ranked comparison of the DMSO-
612 Mon and CHIR-Mon transcriptomes. NES and FDRq values are indicated in each case. **E**. Relative
613 mRNA levels of the indicated genes in monocytes exposed for 16h to DMSO, CHIR-99021 or M-
614 CSF, as determined by RNA-Seq on three independent samples (GSE256538). *Adjp* of the
615 comparison, shown in each case, was assessed using DESeq2. **F**. GSEA of MAFB-regulated gene
616 sets (from GSE155719) on the ranked comparison of the DMSO-Mon and CHIR-Mon
617 transcriptomes. NES and FDRq values are indicated in each case. **G**. Overlap between the genes
618 upregulated (|log2FC|>1; adjp<0.05) in CHIR-Mon (relative to DMSO-Mon) and M-MØ-specific
619 marker genes (from GSE68061) (left panel) and genes downregulated (|log2FC|>1; adjp<0.05) in
620 CHIR-Mon (relative to DMSO-Mon) and GM-MØ-specific marker genes (from GSE68061) (right
621 panel), with indication of some of the overlapping genes. **H**. Schematic representation of the
622 exposure of human monocytes to synovial fluid from rheumatoid arthritis patients (RASF) for 48h
623 in the presence or absence of CHIR-99021. **I**. MAFB protein levels in monocytes exposed to three
624 independent samples of RASF in the presence of DMSO or CHIR-99021, as determined by Western
625 blot (upper panel). Vinculin protein levels were determined as protein loading control. Mean ±
626 SEM of the MAFB/Vinculin protein ratio from seven independent experiments using three
627 monocyte preparations and three unrelated RASF (lower panel) (paired Student's t test: **,
628 p<0.01). **J**. Relative expression of *IL10* and *LGMN* in monocytes exposed to RASF in the presence of

629 DMSO or CHIR-99021, as determined by RT-PCR. Mean ± SEM of the results from the three
630 independent samples are shown (paired Student's t test: **, p<0.01).
631
632 **Figure 6.- Transcriptional and phenotypic effects of GSK3 inhibition on *ex vivo* isolated human**
633 **alveolar macrophages. A**. Schematic representation of the exposure of *ex vivo* isolated human
634 alveolar macrophages to CHIR-99021 or DMSO for 24h. **B**. Volcano plot depicting the differentially
635 expressed genes between CHIR-AMØ and DMSO-AMØ. **C**. Heatmap of the relative expression of
636 the genes within the CD163+/LGMN+ pro-fibrotic monocyte-derived macrophage cluster (from
637 EGAS00001005634) [23] in DMSO-AMØ (lanes A-C) and CHIR-AMØ (lanes D-F). Differentially
638 expressed between CHIR-AMØ and DMSO-AMØ are shown in greeen, and MAFB-dependent genes
639 (GSE155719) are shown in blue. Representative genes are indicated. **D**. (Upper panel) GSEA of the
640 gene sets that characterize the monocyte-derived profibrotic macrophage subsets identified in
641 severe COVID-19, namely CD163+/LGMN+ (EGAS00001005634) [23], MoAM3 (GSE155249) [25] and
642 SPP1+ (GSE145926) [24], on the ranked comparison of the transcriptomes of CHIR-AMØ vs. DMSO-
643 AMØ. NES and FDRq values are indicated in each case. (Lower panel) GSEA of the gene sets that
644 characterize tissue-resident alveolar macrophages in severe COVID-19, namely AMØ1
645 (EGAS00001005634) [23], TRAM1+ (GSE155249) [25] and FABP4+ (GSE145926) [24], on the ranked
646 comparison of the transcriptomes of CHIR-AMØ vs. DMSO-AMØ. **E.** Heatmap of the relative
647 expression of the genes within the Alveolar Macrophage signature (including all the genes
648 overexpressed in the AMØ1 and AMØ2 macrophages clusters from EGAS00001005634) [23] in
649 DMSO-AMØ (lanes A-C) and CHIR-AMØ (lanes D-F). Differentially expressed between CHIR-AMØ
650 and DMSO-AMØ are indicated in greeen, and selected genes are shown. **F**. MAFB protein levels in
651 three independent samples of *ex vivo* isolated AMØ exposed to DMSO or CHIR-99021 for 24h, as
652 determined by Western blot. GAPDH protein levels were determined as protein loading control. **G**.

653 Production of the indicated soluble factors by three independent preparations of DMSO-AMØ and
654 CHIR-AMØ, as determined by ELISA. **H**. Expression of inactive GSK3 (S9, pSer^{9}-GSK3β; S21, pSer^{21}-
655 GSK3α), MAFB and CD163 in human lung macrophages. Representative human lung tissues from
656 COVID (n= 2) and control (n= 3) patients co-stained for CD68 (macrophage marker, red), Ser^{21}-
657 phosphorylated GSK3α, Ser^{9}-phosphorylated GSK3β, MAFB or CD163 (green), and DAPI (nuclei,
658 blue), as indicated (Scale bar, 50 µm) (left panel). Plots show MFI (in arbitrary units, a.u.) of single-
659 cell CD68+ macrophages stained for each antibody (right panel) (paired Student's t test: ****,
660 p<0.001).
661
662 **Figure 7**. **Differential expression of GSK3-regulated genes in human lung interstitial and alveolar**
663 **macrophages. A**. Embedding of 21310 single-cell transcriptomes from human lungs in UMAP
664 (Uniform Manifold Approximation and Projection) with the scVI reduction. Cell-type annotation is
665 based on expression of canonical marker genes, as reported in [47]. **B**. Two-dimensional embedding
666 computed by UMAP with the scVI reduction on computationally identified macrophages after
667 filtering according to number of genes per cell (nFeature, > 200 and < 6000), Unique Molecular
668 Identifiers (nCount, > 1000) and % of mitochondrial genes (< 15 %). **C**. Relative expression of the
669 indicated genes in the four macrophage subsets defined upon re-clustering of the macrophages
670 identified in the single cell RNA sequencing reported in GSE128033 [47]. **D**. Volcano plot illustrating
671 the differentially expressed genes between the Interstitial Macrophage (IMØ) and Alveolar
672 Macrophage (AMØ) subsets defined upon re-analysis of the single cell RNA sequencing reported in
673 GSE128033 [47]. **E-G**. GSEA of the gene sets that define human lung AMØ or IMØ macrophage
674 subsets (GSE128033 and GSE193782) [47,55] on the ranked comparison of CHIR-GM-MØ vs. DMSO-
675 GM-MØ transcriptomes (**E**), CHIR-AMØ vs. DMSO-AMØ transcriptomes (**F**) or siGSK3A/B-GM-MØ
676 vs. siCNT-GM-MØ (**G**).

677

678

679

680 **SUPPLEMENTARY FIGURE LEGENDS**

681 **Figure S1.- A**. MAFB protein levels in GM-MØ exposed to DMSO or distinct CHIR-99021
682 concentrations (0.1μM, 1μM, 10μM) for 6-48 hours, as determined by Western blot (left panel).
683 GAPDH protein levels were determined as protein loading control. Mean ± SEM of the
684 MAFB/GAPDH protein ratio from three independent experiments are shown (right panel) (one-
685 way ANOVA with Fisher LSD test: ***, p<0.005; ****, p<0.001). **B**. p-Ser^{9}-GSK3β and p-Tyr^{216}-
686 GSK3β levels in GM-MØ treated with DMSO, CHIR-99021 (10 μM), SB-216763 (10 μM) or LiCl (10
687 mM) for 48 hours, as determined by Western blot. A representative experiment of three
688 independent experiments is shown in the left panel. GAPDH protein levels were determined as
689 protein loading control. **C**. Gene ontology analysis of the genes upregulated (|log2FC|>1;
690 adjp<0.05) in CHIR-GM-MØ (relative to DMSO GM-MØ) using Enrichr and the indicated databases.
691 **D**. Oxygen Consumption rate (OCR) profile of DMSO-GM-MØ and CHIR-GM-MØ monitored using
692 the Seahorse Biosciences extracellular flux analyzer at the indicated time points. Cells were
693 treated sequentially, as indicated, with 1 mM oligomycin (Oligo), 0.6 plus 0.4 mM FCCP, and 1 mM
694 rotenone plus 1 mM antimycin A (Rot/AA). **E**. Extracellular acidification rate (ECAR), a proxy for
695 the rate of lactate production, measured in DMSO-GM-MØ and CHIR-GM-MØ under basal
696 conditions and after the stimulation with 1 mM oligomycin and at the indicated time points. **F**.
697 Metabolic parameters obtained from the OCR and ECAR profiling after subtraction of the
698 rotenone/antimycin-insensitive respiration. Basal OCR is the oxygen consumption rate in the
699 absence of effectors, ATP turnover is considered as the oligomycin-sensitive respiration, maximal
700 respiration is the OCR value in the presence of the uncoupler FCCP, glycolytic capacity is the ECAR

701 value after the inhibition with oligomycin of the mitochondrial ATP synthesis (paired Student's t
702 test: ***, p<0.005; n.s., not significant). In **D-F**, results are normalized according to protein
703 concentrations and presented as mean ± SEM of six independent samples.
704
705 **Figure S2. A**. Summary of GSEA of the gene sets that characterize the macrophage subsets
706 identified in severe COVID-19 [23–25] on the ranked comparison of siGSK3A-GM-MØ vs. siCNT-GM-
707 MØ (square symbols), siGSK3B-GM-MØ vs. siCNT-GM-MØ (star symbols) and siGSK3A/B-GM-MØ
708 vs. siCNT-GM-MØ. FDRq values are indicated only if FDRq>0.0; empty dots, Not Significant. **B.**
709 GSEA of *bona fide* MAFB-bound genes ("75-genelist") [52] on the ranked comparison of the
710 transcriptomes of CHIR-Mon vs DMSO-Mon. NES and FDRq value is indicated. **C**. Summary of GSEA
711 of the gene sets that characterize the macrophage subsets identified in severe COVID-19 [23–25] on
712 the ranked comparison of the transcriptomes of CHIR-Mon vs. DMSO-Mon. FDRq values are
713 indicated only if FDRq>0.0; empty dots, Not Significant. **D**. Overlap between the genes upregulated
714 (|log2FC|>1; adjp<0.05) in CHIR-Mon (relative to M-CSF-Mon) and M-MØ-specific marker genes
715 (left panel) and genes downregulated (|log2FC|>1; adjp<0.05) in CHIR-Mon (relative to M-CSF-
716 Mon) and GM-MØ-specific marker genes (right panel), with indication of some shared genes. **E.**
717 Overlap between the genes upregulated or downregulated in CHIR-AMØ (|log2FC|>1 and
718 adjp<0.05) and the CD163+/LGMN+ pro-fibrotic macrophage cluster defined in EGAS00001005634
719 [23] (left panel), or the gene sets of MAFB-dependent (middle panel) and MAFB-inhibited (right
720 panel) genes defined in GSE155719 [52]. **F**. Overlap between the genes upregulated or
721 downregulated in CHIR-AMØ (|log2FC|>1 and adjp<0.05, or just adjp<0.05) and the Alveolar
722 Macrophage signature as defined in EGAS00001005634 (AMØ1 and AMØ2 clusters) [23] (left panel),
723 GSE155249 (TRAM1 and TRAM2 clusters) [25] (middle panel) or in [54] (right panel). **G.** Summary of

724 GSEA of the indicated gene sets (from GSE68061 and GSE188278) on the ranked comparison of
725 the DMSO-AMØ and CHIR-AMØ transcriptomes. FDRq values are indicated only if FDRq>0.0.
726
727 **Figure S3**. **A**. Number of cells from single cell-RNA sequencing on human lungs from eight
728 independent donors (from GSE128033) [47], after filtering according to number of genes per cell
729 (nFeature, > 200 and < 6000), Unique Molecular Identifiers (nCount, > 1000) and % of
730 mitochondrial genes (< 15 %). **B**. UMAP (Uniform Manifold Approximation and Projection), with
731 the scVI reduction, embedding of 21310 single-cell transcriptomes from human lungs as reported
732 in GSE128033 [47], with color-coding indicating distinct cell clusters. **C**. UMAP (Uniform Manifold
733 Approximation and Projection), with the scVI reduction, embedding of 21310 single-cell
734 transcriptomes from human lungs as reported in GSE128033 [47], with color-coding indicating donor
735 origin. **D**. Color-coded expression of the indicated genes after projection onto the UMAP
736 embedding shown in **B-C**.
737
738 **Figure S4**. **A**. UMAP (Uniform Manifold Approximation and Projection), with the scVI reduction,
739 embedding of single-cell transcriptomes from human lung macrophages as reported in GSE128033
740 [47], with color-coding indicating distinct cell clusters. **B**. UMAP (Uniform Manifold Approximation
741 and Projection), with the scVI reduction, embedding of single-cell transcriptomes from human
742 lungs as reported in GSE128033 [47], with color-coding indicating donor origin. **C**. Color-coded
743 expression of the genes used for macrophage definition (*CD163*, *FABP4*, *LYVE1, FCN1*), as well as
744 proliferation-associated genes (*TYMS, MKI67*, *TOP2A*, *NUSAP1*) and other *bona fide* macrophage
745 marker genes (*SPI1*, *FOLR2*), after projection onto the UMAP embedding shown in **B-C**.
746
747 **SUPPLEMENTARY TABLES**

748 **Table S1**.- Transcriptional datasets used in the present study.

749

750 **REFERENCES**

751 1. Dick, S. A. *et al.* Three tissue resident macrophage subsets coexist across organs with
752 conserved origins and life cycles. *Sci. Immunol.* **7**, (2022).
753 2. Mulder, K. *et al.* Cross-tissue single-cell landscape of human monocytes and
754 macrophages in health and disease. *Immunity* **54**, 1883-1900.e5 (2021).
755 3. Hoeffel, G. & Ginhoux, F. Fetal monocytes and the origins of tissue-resident
756 macrophages. *Cell. Immunol.* **330**, 5–15 (2018).
757 4. Ruffell, B. & Coussens, L. M. Macrophages and therapeutic resistance in cancer.
758 *Cancer Cell* **27**, 462–472 (2015).
759 5. Lavin, Y., Mortha, A., Rahman, A. & Merad, M. Regulation of macrophage
760 development and function in peripheral tissues. *Nat Rev Immunol* **15**, 731–744 (2015).
761 6. Caescu, C. I. *et al.* Colony stimulating factor-1 receptor signaling networks inhibit
762 mouse macrophage inflammatory responses by induction of microRNA-21. *Blood* **125**,
763 e1–e13 (2015).
764 7. Van Overmeire, E. *et al.* M-CSF and GM-CSF Receptor Signaling Differentially Regulate
765 Monocyte Maturation and Macrophage Polarization in the Tumor Microenvironment.
766 *Cancer Res* **76**, 35–42 (2016).
767 8. Fleetwood, A. J., Lawrence, T., Hamilton, J. A. & Cook, A. D. Granulocyte-Macrophage
768 Colony-Stimulating Factor (CSF) and Macrophage CSF-Dependent Macrophage
769 Phenotypes Display Differences in Cytokine Profiles and Transcription Factor
770 Activities: Implications for CSF Blockade in Inflammation. *J. Immunol.* **178**, 5245–5252
771 (2007).
772 9. Lacey, D. C. *et al.* Defining GM-CSF- and Macrophage-CSF-Dependent Macrophage
773 Responses by In Vitro Models. *J Immunol* **188**, 5752–5765 (2012).
774 10. Gonzalez-Dominguez, E. *et al.* Atypical Activin A and IL-10 Production Impairs Human
775 CD16+ Monocyte Differentiation into Anti-Inflammatory Macrophages. *J Immunol*
776 **196**, 1327–1337 (2016).
777 11. Fleetwood, A. J., Dinh, H., Cook, A. D., Hertzog, P. J. & Hamilton, J. A. GM-CSF- and M-
778 CSF-dependent macrophage phenotypes display differential dependence on Type I
779 interferon signaling. *J. Leukoc. Biol.* **86**, 411–421 (2009).
780 12. Sierra-Filardi, E. *et al.* Activin A skews macrophage polarization by promoting a

781 proinflammatory phenotype and inhibiting the acquisition of anti-inflammatory
782 macrophage markers. *Blood* **117**, 5092–5101 (2011).
783 13. Gonzalez-Dominguez, E. *et al.* CD163L1 and CLEC5A discriminate subsets of human
784 resident and inflammatory macrophages in vivo. *J. Leukoc. Biol.* **98**, 453–466 (2015).
785 14. Palacios, B. S. *et al.* Macrophages from the synovium of active rheumatoid arthritis
786 exhibit an activin a-dependent pro-inflammatory profile. *J. Pathol.* **235**, 515–526
787 (2015).
788 15. de las Casas-Engel, M. *et al.* Serotonin Skews Human Macrophage Polarization
789 through HTR 2B and HTR 7 . *J. Immunol.* **190**, 2301–2310 (2013).
790 16. Nieto, C. *et al.* The activin A-peroxisome proliferator-activated receptor gamma axis
791 contributes to the transcriptome of GM-CSF-conditioned human macrophages. *Front.*
792 *Immunol.* **9**, (2018).
793 17. Guilliams, M. *et al.* Alveolar macrophages develop from fetal monocytes that
794 differentiate into long-lived cells in the first week of life via GM-CSF. *J Exp Med* **210**,
795 1977–1992 (2013).
796 18. Trapnell, B. C., Carey, B. C., Uchida, K. & Suzuki, T. Pulmonary alveolar proteinosis, a
797 primary immunodeficiency of impaired GM-CSF stimulation of macrophages. *Curr*
798 *Opin Immunol* **21**, 514–521 (2009).
799 19. Huang, X., Cao, M. & Xiao, Y. Alveolar macrophages in pulmonary alveolar proteinosis:
800 origin, function, and therapeutic strategies. *Front. Immunol.* **14**, (2023).
801 20. Donadon, M. *et al.* Macrophage morphology correlates with single-cell diversity and
802 prognosis in colorectal liver metastasis. *J. Exp. Med.* **217**, (2020).
803 21. Joshi, N. *et al.* A spatially restricted fibrotic niche in pulmonary fibrosis is sustained by
804 M-CSF/M-CSFR signalling in monocyte-derived alveolar macrophages. *Eur. Respir. J.*
805 **55**, 1–16 (2020).
806 22. Vega, M. A. *et al.* MAFB and MAF Transcription Factors as Macrophage Checkpoints
807 for COVID-19 Severity. *Front. Immunol.* **11**, (2020).
808 23. Wendisch, D. *et al.* SARS-CoV-2 infection triggers profibrotic macrophage responses
809 and lung fibrosis. *Cell* **184**, 6243-6261.e27 (2021).
810 24. Liao, M. *et al.* Single-cell landscape of bronchoalveolar immune cells in patients with
811 COVID-19. *Nat. Med.* **26**, 842–844 (2020).

812 25. Grant, R. A. *et al.* Circuits between infected macrophages and T cells in SARS-CoV-2
813 pneumonia. *Nature* **590**, 635–641 (2021).
814 26. Schultze, J. L. Reprogramming of macrophages - New opportunities for therapeutic
815 targeting. *Curr. Opin. Pharmacol.* **26**, 10–15 (2016).
816 27. Cuevas, V. D. *et al.* MAFB Determines Human Macrophage Anti-Inflammatory
817 Polarization: Relevance for the Pathogenic Mechanisms Operating in Multicentric
818 Carpotarsal Osteolysis. *J. Immunol.* **198**, 2070–2081 (2017).
819 28. Kim, H. The transcription factor MafB promotes anti-inflammatory M2 polarization
820 and cholesterol efflux in macrophages. *Sci. Rep.* **7**, (2017).
821 29. Kang, K. *et al.* Interferon-γ Represses M2 Gene Expression in Human Macrophages by
822 Disassembling Enhancers Bound by the Transcription Factor MAF. *Immunity* **47**, 235-
823 250.e4 (2017).
824 30. Eychène, A., Rocques, N. & Pouponnot, C. A new MAFia in cancer. *Nature Reviews*
825 *Cancer* vol. 8 683–693 (2008).
826 31. Lavin, Y. *et al.* Tissue-resident macrophage enhancer landscapes are shaped by the
827 local microenvironment. *Cell* **159**, 1312–1326 (2014).
828 32. Kelly, L. M., Englmeier, U., Lafon, I., Sieweke, M. H. & Graf, T. MafB is an inducer of
829 monocytic differentiation. *EMBO J.* **19**, 1987–1997 (2000).
830 33. Aziz, A., Soucie, E., Sarrazin, S. & Sieweke, M. H. MafB/c-Maf deficiency enables self-
831 renewal of differentiated functional macrophages. *Science (80-.).* **326**, 867–871
832 (2009).
833 34. Soucie, E. L. *et al.* Lineage-specific enhancers activate self-renewal genes in
834 macrophages and embryonic stem cells. *Science (80-.).* **351**, aad5510 (2016).
835 35. Sarrazin, S. *et al.* MafB restricts M-CSF-dependent myeloid commitment divisions of
836 hematopoietic stem cells. *Cell* **138**, 300–313 (2009).
837 36. Cuevas, V. D. *et al.* The gene signature of activated M-CSF-Primed human monocyte-
838 derived macrophages is IL-10-dependent. *J. Innate Immun.* (2021)
839 doi:10.1159/000519305.
840 37. Ríos, I. *et al.* GSK3β Inhibition Prevents Macrophage Reprogramming by High-Dose
841 Methotrexate. *J. Innate Immun.* **15**, 283–296 (2022).
842 38. de la Aleja, A. G. *et al.* Inhibition of LXR controls the polarization of human

843 inflammatory macrophages through upregulation of MAFB. *Cell. Mol. Life Sci.* **80**,
844 (2023).
845 39. Nagayoshi, R. *et al.* Effectiveness of anti-folate receptor β antibody conjugated with
846 truncated Pseudomonas exotoxin in the targeting of rheumatoid arthritis synovial
847 macrophages. *Arthritis Rheum.* **52**, 2666–2675 (2005).
848 40. Kim, D., Paggi, J. M., Park, C., Bennett, C. & Salzberg, S. L. Graph-based genome
849 alignment and genotyping with HISAT2 and HISAT-genotype. *Nat. Biotechnol.* **37**, 907–
850 915 (2019).
851 41. Langmead, B. & Salzberg, S. L. Fast gapped-read alignment with Bowtie 2. *Nat.*
852 *Methods* **9**, 357–359 (2012).
853 42. Anders, S., Pyl, P. T. & Huber, W. HTSeq-A Python framework to work with high-
854 throughput sequencing data. *Bioinformatics* **31**, 166–169 (2015).
855 43. Li, B. & Dewey, C. N. RSEM: Accurate transcript quantification from RNA-Seq data with
856 or without a reference genome. *BMC Bioinformatics* **12**, (2011).
857 44. Chen, E. Y. *et al.* Enrichr: Interactive and collaborative HTML5 gene list enrichment
858 analysis tool. *BMC Bioinformatics* **14**, 128 (2013).
859 45. Kuleshov, M. V *et al.* Enrichr: a comprehensive gene set enrichment analysis web
860 server 2016 update. *Nucleic Acids Res* **44**, W90–W97 (2016).
861 46. Subramanian, A. *et al.* Gene set enrichment analysis: a knowledge-based approach for
862 interpreting genome-wide expression profiles. *Proc Natl Acad Sci U S A* **102**, 15545–
863 15550 (2005).
864 47. Morse, C. *et al.* Proliferating SPP1/MERTK-expressing macrophages in idiopathic
865 pulmonary fibrosis. *Eur. Respir. J.* **54**, (2019).
866 48. Brand, M. D. & Nicholls, D. G. Assessing mitochondrial dysfunction in cells. *Biochem. J.*
867 **435**, 297–312 (2011).
868 49. Rueden, C. T. *et al.* ImageJ2: ImageJ for the next generation of scientific image data.
869 *BMC Bioinformatics* **18**, (2017).
870 50. Gutiérrez-Seijo, A. *et al.* Activin A Sustains the Metastatic Phenotype of Tumor-
871 Associated Macrophages and Is a Prognostic Marker in Human Cutaneous Melanoma.
872 *J. Invest. Dermatol.* **142**, 653-661.e2 (2022).
873 51. Garcia-Alonso, L., Holland, C. H., Ibrahim, M. M., Turei, D. & Saez-Rodriguez, J.

874 Benchmark and integration of resources for the estimation of human transcription
875 factor activities. *Genome Res.* **29**, 1363–1375 (2019).
876 52. Simón-Fuentes, M. *et al.* MAFB shapes human monocyte–derived macrophage
877 response to SARS-CoV-2 and controls severe COVID-19 biomarker expression. *JCI*
878 *Insight* **8**, (2023).
879 53. Wculek, S. K., Dunphy, G., Heras-Murillo, I., Mastrangelo, A. & Sancho, D. Metabolism
880 of tissue macrophages in homeostasis and pathology. *Cellular and Molecular*
881 *Immunology* vol. 19 384–408 (2022).
882 54. Melms, J. C. *et al.* A molecular single-cell lung atlas of lethal COVID-19. *Nature* **595**,
883 (2021).
884 55. Li, X. *et al.* ScRNA-seq expression of IFI27 and APOC2 identifies four alveolar
885 macrophage superclusters in healthy BALF. *Life Sci. Alliance* **5**, (2022).
886 56. González de la Aleja, A. *et al.* Activation of LXR Nuclear Receptors Impairs the Anti-
887 Inflammatory Gene and Functional Profile of M-CSF-Dependent Human Monocyte-
888 Derived Macrophages. *Front. Immunol.* **13**, (2022).
889 57. Domínguez-Soto, Á. *et al.* IVIg Promote Cross-Tolerance against Inflammatory Stimuli
890 In Vitro and In Vivo. *J. Immunol.* **201**, 41–52 (2018).
891 58. Molgora, M. & Colonna, M. Turning enemies into allies—reprogramming tumor-
892 associated macrophages for cancer therapy. *Med* vol. 2 666–681 (2021).
893 59. Zheng, W. & Pollard, J. W. Inhibiting macrophage PI3K? To enhance immunotherapy.
894 *Cell Res.* **26**, 1267–1268 (2016).
895 60. Kaneda, M. M. *et al.* PI3Kγ 3 is a molecular switch that controls immune suppression.
896 *Nature* **539**, 437–442 (2016).
897 61. Byles, V. *et al.* The TSC-mTOR pathway regulates macrophage polarization. *Nat.*
898 *Commun.* **4**, (2013).
899 62. Do, M. H. *et al.* Reprogramming tumor-associated macrophages to outcompete
900 endovascular endothelial progenitor cells and suppress tumor neoangiogenesis.
901 *Immunity* **56**, 2555-2569.e5 (2023).
902 63. Zhang, X. *et al.* Reprogramming tumour-associated macrophages to outcompete
903 cancer cells. *Nature* **619**, 616–623 (2023).
904 64. Evangelisti, C., Chiarini, F., Paganelli, F., Marmiroli, S. & Martelli, A. M. Crosstalks of

905 GSK3 signaling with the mTOR network and effects on targeted therapy of cancer.
906 *Biochimica et Biophysica Acta - Molecular Cell Research* vol. 1867 (2020).
907 65. Rodionova, E. *et al.* GSK-3 mediates differentiation and activation of proinflammatory
908 dendritic cells. *Blood* **109**, 1584–1592 (2007).
909 66. Bakri, Y. *et al.* Balance of MafB and PU.1 specifies alternative macrophage or dendritic
910 cell fate. *Blood* **105**, 2707–2716 (2005).
911 67. Delorey, T. M. *et al.* COVID-19 tissue atlases reveal SARS-CoV-2 pathology and cellular
912 targets. *Nature* **595**, 107–113 (2021).
913 68. Koshida, R., Oishi, H., Hamada, M. & Takahashi, S. MafB antagonizes phenotypic
914 alteration induced by GM-CSF in microglia. *Biochem Biophys Res Commun* **463**, 109–
915 115 (2015).
916 69. Lang, F. M., Lee, K. M. C., Teijaro, J. R., Becher, B. & Hamilton, J. A. GM-CSF-based
917 treatments in COVID-19: reconciling opposing therapeutic approaches. *Nat. Rev.*
918 *Immunol.* (2020) doi:10.1038/s41577-020-0357-7.
919 70. Bosteels, C. *et al.* Loss of GM-CSF-dependent instruction of alveolar macrophages in
920 COVID-19 provides a rationale for inhaled GM-CSF treatment. *Cell Reports Med.* **3**,
921 (2022).
922

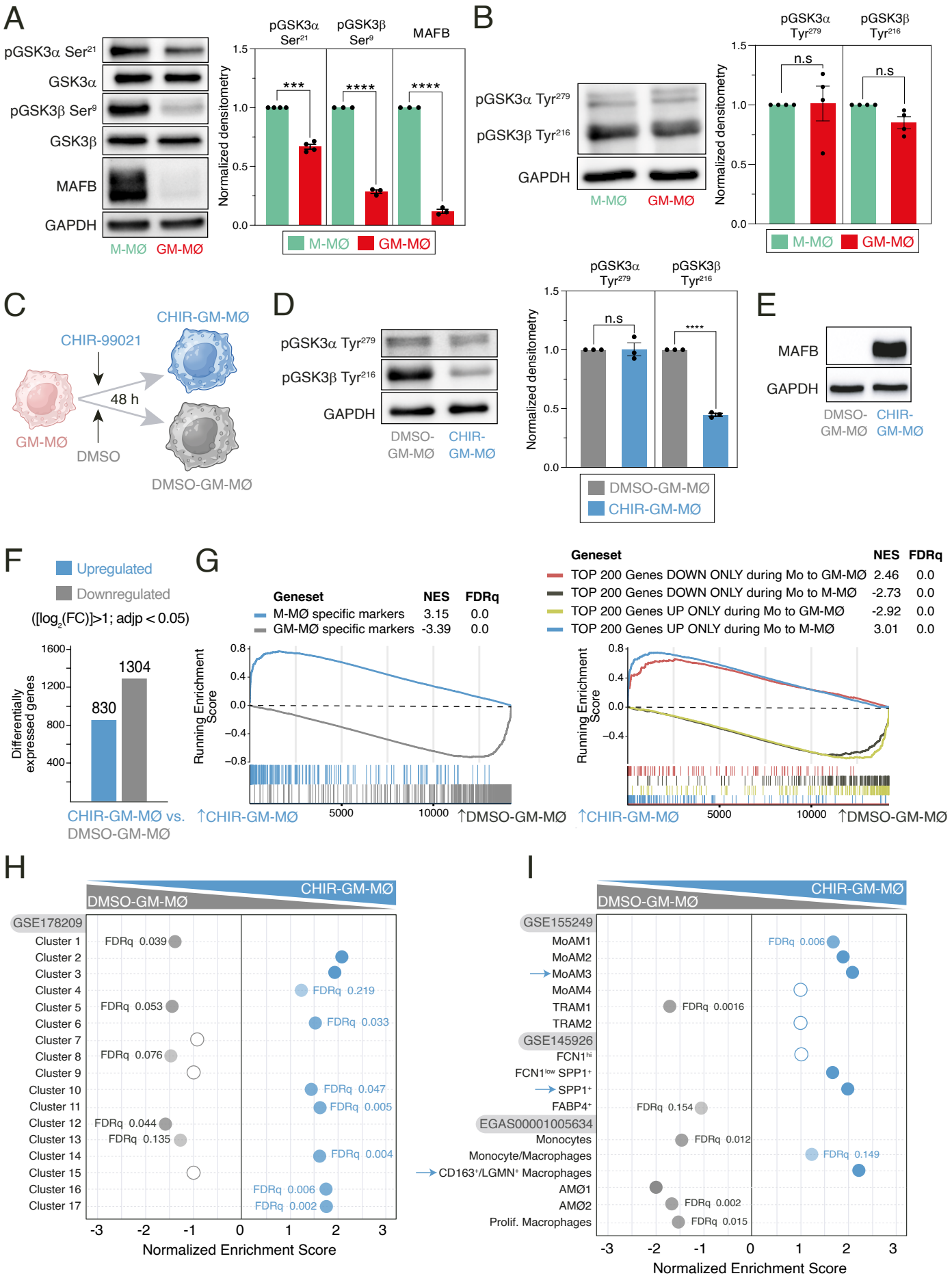
A
pGSK3α Ser21
GSK3α
pGSK3β Ser9
GSK3β
MAFB
GAPDH
M-MØ GM-MØ
pGSK3α Ser21
pGSK3β Ser9
MAFB
Normalized densitometry
***
****
****
M-MØ GM-MØ
B
pGSK3α Tyr279
pGSK3β Tyr216
GAPDH
M-MØ GM-MØ
pGSK3α Tyr279
pGSK3β Tyr216
n.s
n.s
Normalized densitometry
M-MØ GM-MØ
C
CHIR-GM-MØ
CHIR-99021
48 h
GM-MØ
DMSO
DMSO-GM-MØ
D
pGSK3α Tyr279
pGSK3β Tyr216
GAPDH
DMSO-GM-MØ
CHIR-GM-MØ
pGSK3α Tyr279
pGSK3β Tyr216
n.s
****
Normalized densitometry
DMSO-GM-MØ
CHIR-GM-MØ
E
MAFB
GAPDH
DMSO-GM-MØ
CHIR-GM-MØ
F
Upregulated
Downregulated
([log2(FC)]>1; adjp < 0.05)
Differentially expressed genes
830
1304
CHIR-GM-MØ vs. DMSO-GM-MØ
G
Geneset NES FDRq
M-MØ specific markers 3.15 0.0
GM-MØ specific markers -3.39 0.0
Running Enrichment Score
↑CHIR-GM-MØ
↑DMSO-GM-MØ
Geneset NES FDRq
TOP 200 Genes DOWN ONLY during Mo to GM-MØ 2.46 0.0
TOP 200 Genes DOWN ONLY during Mo to M-MØ -2.73 0.0
TOP 200 Genes UP ONLY during Mo to GM-MØ -2.92 0.0
TOP 200 Genes UP ONLY during Mo to M-MØ 3.01 0.0
Running Enrichment Score
↑CHIR-GM-MØ
↑DMSO-GM-MØ
H
CHIR-GM-MØ
DMSO-GM-MØ
GSE178209
Cluster 1 FDRq 0.039
Cluster 2
Cluster 3
Cluster 4 FDRq 0.219
Cluster 5 FDRq 0.053
Cluster 6 FDRq 0.033
Cluster 7
Cluster 8 FDRq 0.076
Cluster 9
Cluster 10 FDRq 0.047
Cluster 11 FDRq 0.005
Cluster 12 FDRq 0.044
Cluster 13 FDRq 0.135
Cluster 14 FDRq 0.004
Cluster 15
Cluster 16 FDRq 0.006
Cluster 17 FDRq 0.002
Normalized Enrichment Score
I
CHIR-GM-MØ
DMSO-GM-MØ
GSE155249
MoAM1 FDRq 0.006
MoAM2
MoAM3
MoAM4
TRAM1 FDRq 0.0016
TRAM2
GSE145926
FCN1hi
FCN1low SPP1+
SPP1+
FABP4+ FDRq 0.154
EGAS00001005634
Monocytes FDRq 0.012
Monocyte/Macrophages FDRq 0.149
CD163+/LGMN+ Macrophages
AMØ1
AMØ2 FDRq 0.002
Prolif. Macrophages FDRq 0.015
Normalized Enrichment Score

Figure 1

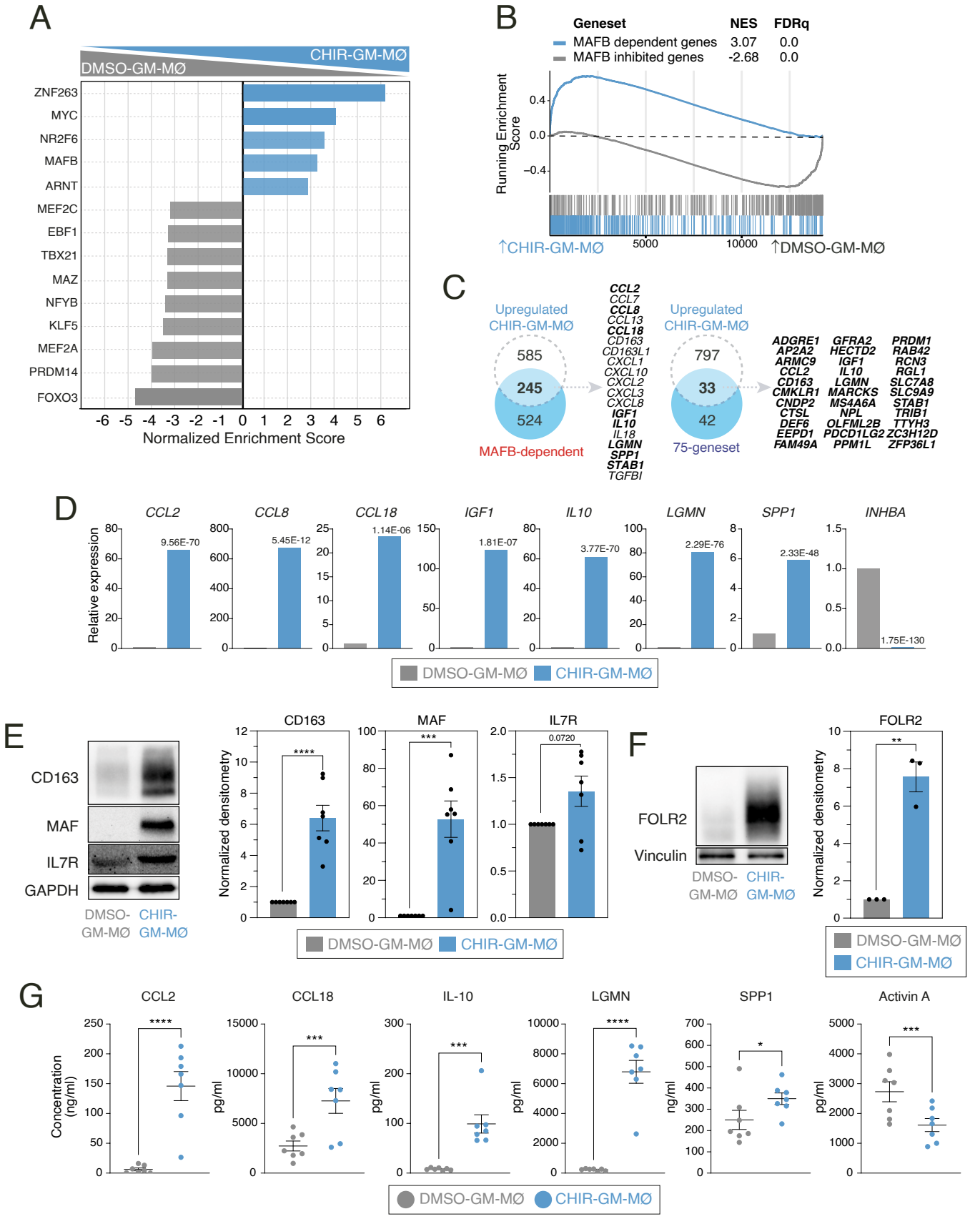
A
CHIR-GM-MØ
DMSO-GM-MØ
ZNF263
MYC
NR2F6
MAFB
ARNT
MEF2C
EBF1
TBX21
MAZ
NFYB
KLF5
MEF2A
PRDM14
FOXO3
-6 -5 -4 -3 -2 -1 0 1 2 3 4 5 6
Normalized Enrichment Score
B
Geneset NES FDRq
MAFB dependent genes 3.07 0.0
MAFB inhibited genes -2.68 0.0
Running Enrichment Score
0.4
0.0
−0.4
↑CHIR-GM-MØ
5000
10000
↑DMSO-GM-MØ
C
Upregulated CHIR-GM-MØ
585
245
524
MAFB-dependent
CCL2 CCL7 CCL8 CCL13 CCL18 CD163 CD163L1 CXCL1 CXCL10 CXCL2 CXCL3 CXCL8 IGF1 IL10 IL18 LGMN SPP1 STAB1 TGFBI
Upregulated CHIR-GM-MØ
797
33
42
75-geneset
ADGRE1 AP2A2 ARMC9 CCL2 CD163 CMKLR1 CNDP2 CTSL DEF6 EEPD1 FAM49A
GFRA2 HECTD2 IGF1 IL10 LGMN MARCKS MS4A6A NPL OLFML2B PDCD1LG2 PPM1L
PRDM1 RAB42 RCN3 RGL1 SLC7A8 SLC9A9 STAB1 TRIB1 TTYH3 ZC3H12D ZFP36L1
D
CCL2 CCL8 CCL18 IGF1 IL10 LGMN SPP1 INHBA
Relative expression
9.56E-70
5.45E-12
1.14E-06
1.81E-07
3.77E-70
2.29E-76
2.33E-48
1.75E-130
DMSO-GM-MØ CHIR-GM-MØ
E
CD163
MAF
IL7R
GAPDH
DMSO-GM-MØ CHIR-GM-MØ
CD163 MAF IL7R
Normalized densitometry
****
***
0.0720
DMSO-GM-MØ CHIR-GM-MØ
F
FOLR2
Vinculin
DMSO-GM-MØ CHIR-GM-MØ
FOLR2
Normalized densitometry
**
DMSO-GM-MØ
CHIR-GM-MØ
G
CCL2 CCL18 IL-10 LGMN SPP1 Activin A
Concentration (ng/ml)
pg/ml
ng/ml
****
***
*
DMSO-GM-MØ CHIR-GM-MØ

Figure 2

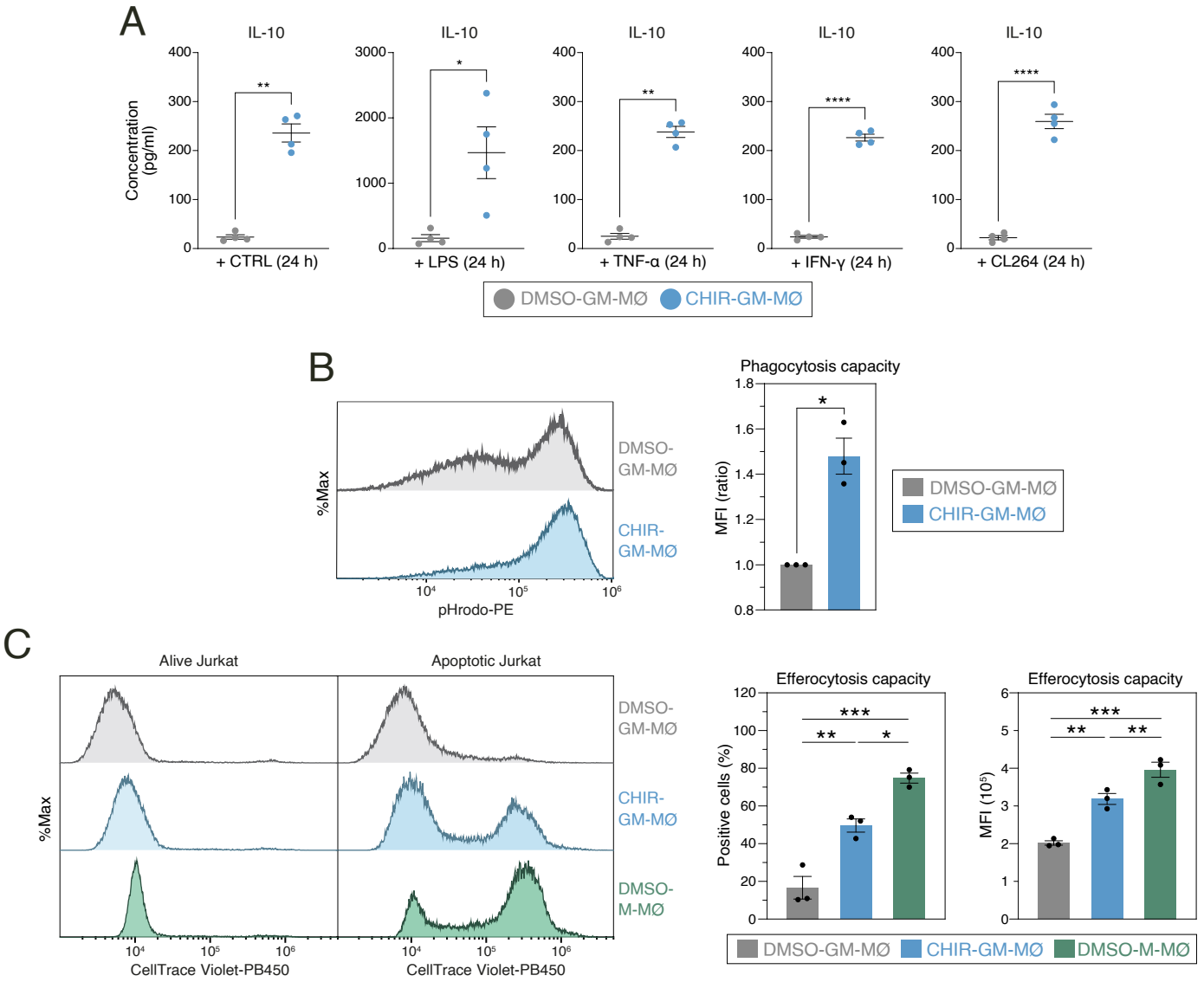
A
IL-10
Concentration (pg/ml)
+ CTRL (24 h)
+ LPS (24 h)
+ TNF-α (24 h)
+ IFN-γ (24 h)
+ CL264 (24 h)
DMSO-GM-MØ
CHIR-GM-MØ
B
%Max
pHrodo-PE
Phagocytosis capacity
MFI (ratio)
C
Alive Jurkat
Apoptotic Jurkat
CellTrace Violet-PB450
Efferocytosis capacity
Positive cells (%)
MFI (10⁵)
DMSO-M-MØ

Figure 3

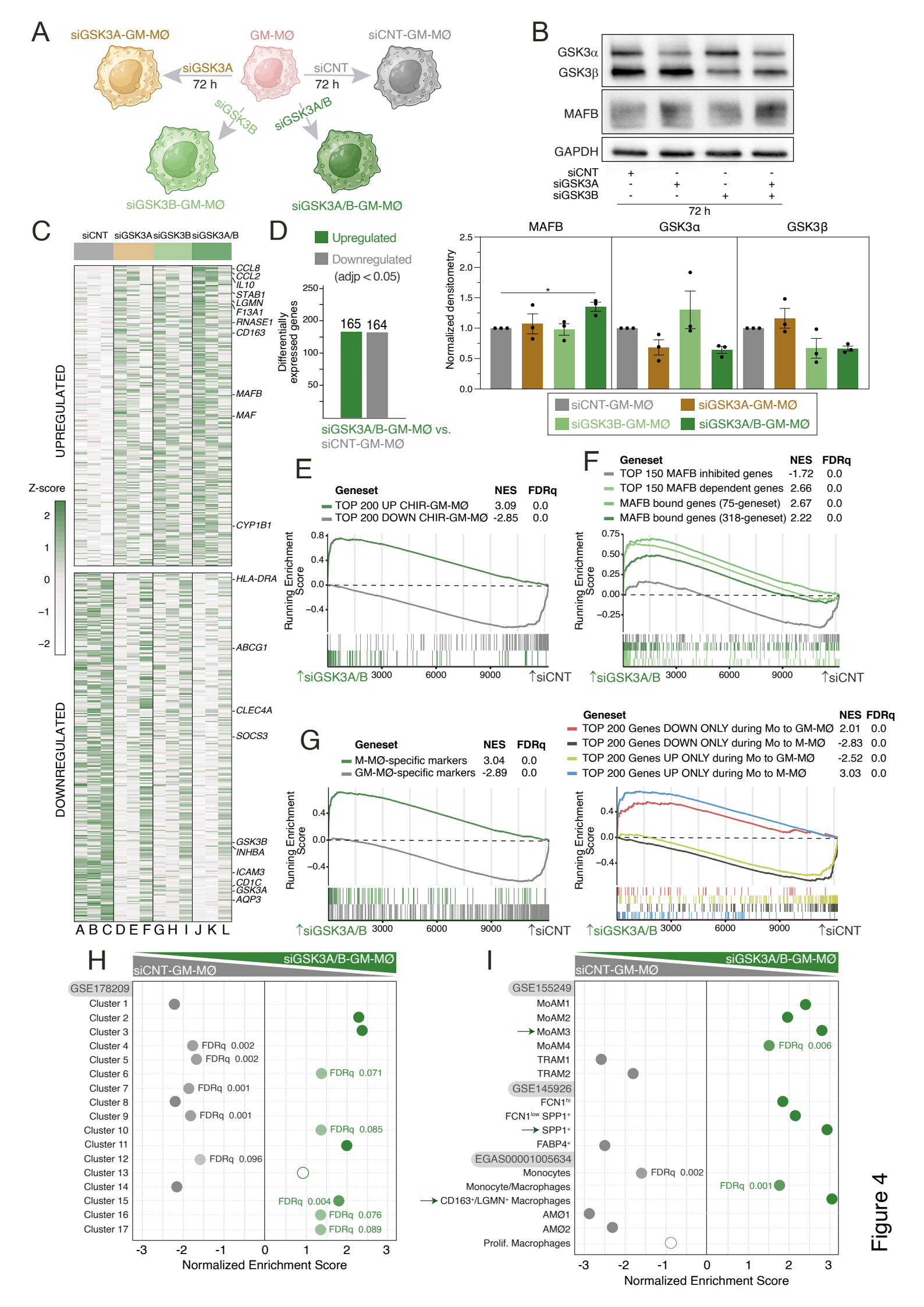
A
siGSK3A-GM-MØ
GM-MØ
siCNT-GM-MØ
siGSK3A
72 h
siCNT
72 h
siGSK3B
siGSK3A/B
siGSK3B-GM-MØ
siGSK3A/B-GM-MØ
B
GSK3α
GSK3β
MAFB
GAPDH
siCNT
siGSK3A
siGSK3B
72 h
C
siCNT siGSK3A siGSK3B siGSK3A/B
UPREGULATED
DOWNREGULATED
Z-score
CCL8
CCL2
IL10
STAB1
LGMN
F13A1
RNASE1
CD163
MAFB
MAF
CYP1B1
HLA-DRA
ABCG1
CLEC4A
SOCS3
GSK3B
INHBA
ICAM3
CD1C
GSK3A
AQP3
A B C D E F G H I J K L
D
Upregulated
Downregulated
(adjp < 0.05)
Differentially expressed genes
165 164
siGSK3A/B-GM-MØ vs. siCNT-GM-MØ
MAFB
GSK3α
GSK3β
Normalized densitometry
siCNT-GM-MØ
siGSK3A-GM-MØ
siGSK3B-GM-MØ
siGSK3A/B-GM-MØ
E
Geneset NES FDRq
TOP 200 UP CHIR-GM-MØ 3.09 0.0
TOP 200 DOWN CHIR-GM-MØ -2.85 0.0
Running Enrichment Score
↑siGSK3A/B
↑siCNT
F
Geneset NES FDRq
TOP 150 MAFB inhibited genes -1.72 0.0
TOP 150 MAFB dependent genes 2.66 0.0
MAFB bound genes (75-geneset) 2.67 0.0
MAFB bound genes (318-geneset) 2.22 0.0
Running Enrichment Score
↑siGSK3A/B
↑siCNT
G
Geneset NES FDRq
M-MØ-specific markers 3.04 0.0
GM-MØ-specific markers -2.89 0.0
Geneset NES FDRq
TOP 200 Genes DOWN ONLY during Mo to GM-MØ 2.01 0.0
TOP 200 Genes DOWN ONLY during Mo to M-MØ -2.83 0.0
TOP 200 Genes UP ONLY during Mo to GM-MØ -2.52 0.0
TOP 200 Genes UP ONLY during Mo to M-MØ 3.03 0.0
Running Enrichment Score
↑siGSK3A/B
↑siCNT
H
siCNT-GM-MØ
siGSK3A/B-GM-MØ
GSE178209
Cluster 1
Cluster 2
Cluster 3
Cluster 4 FDRq 0.002
Cluster 5 FDRq 0.002
Cluster 6 FDRq 0.071
Cluster 7 FDRq 0.001
Cluster 8
Cluster 9 FDRq 0.001
Cluster 10 FDRq 0.085
Cluster 11
Cluster 12 FDRq 0.096
Cluster 13
Cluster 14
Cluster 15 FDRq 0.004
Cluster 16 FDRq 0.076
Cluster 17 FDRq 0.089
Normalized Enrichment Score
I
siCNT-GM-MØ
siGSK3A/B-GM-MØ
GSE155249
MoAM1
MoAM2
MoAM3
MoAM4 FDRq 0.006
TRAM1
TRAM2
GSE145926
FCN1hi
FCN1low SPP1+
SPP1+
FABP4+
EGAS00001005634
Monocytes FDRq 0.002
Monocyte/Macrophages FDRq 0.001
CD163+/LGMN+ Macrophages
AMØ1
AMØ2
Prolif. Macrophages
Normalized Enrichment Score
Figure 4

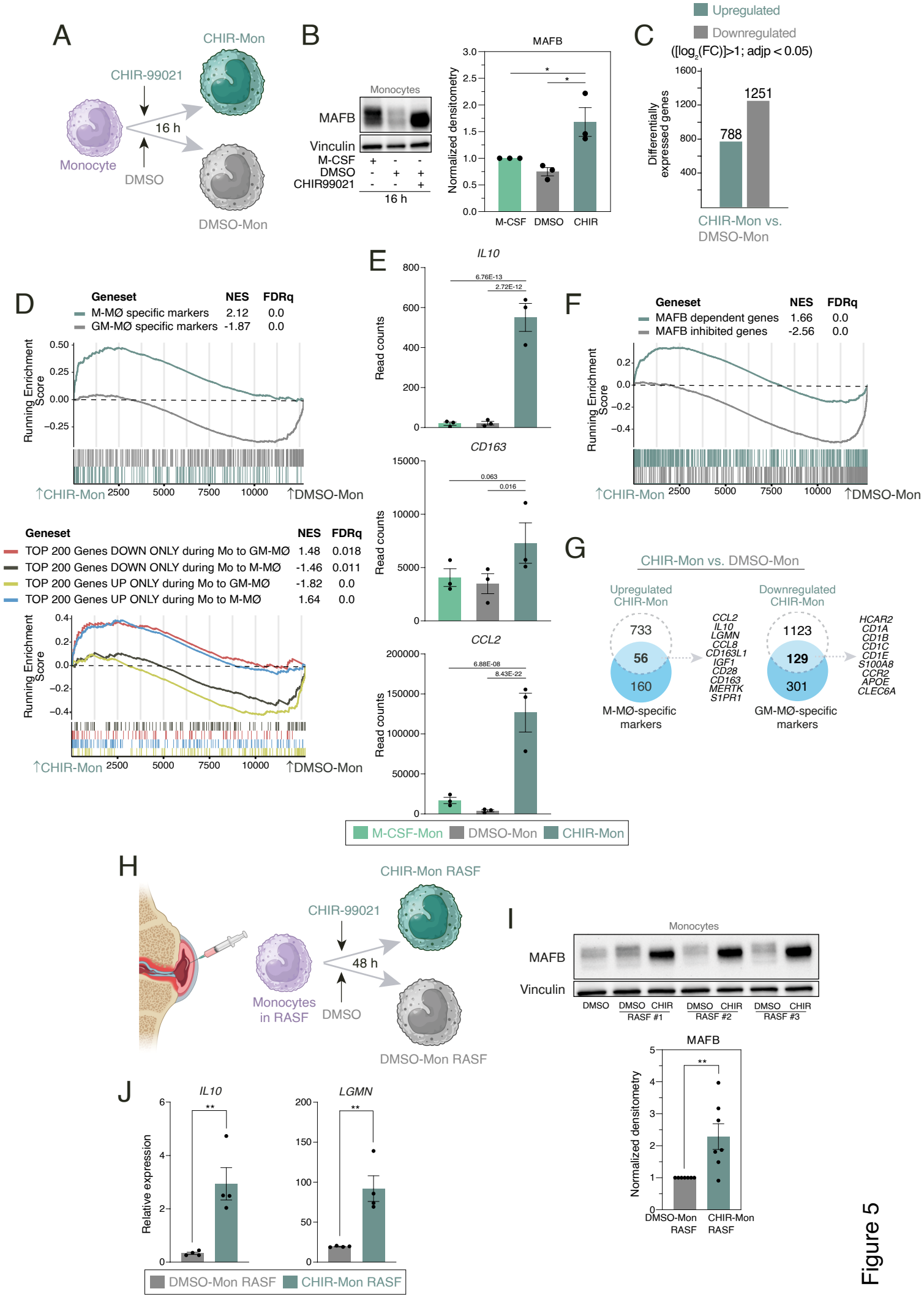
A
CHIR-Mon
CHIR-99021
16 h
Monocyte
DMSO
DMSO-Mon
B
Monocytes
MAFB
Vinculin
M-CSF + - -
DMSO - + +
CHIR99021 - - +
16 h
MAFB
Normalized densitometry
M-CSF DMSO CHIR
C
Upregulated
Downregulated
([log2(FC)]>1; adjp < 0.05)
Differentially expressed genes
788
1251
CHIR-Mon vs. DMSO-Mon
D
Geneset NES FDRq
M-MØ specific markers 2.12 0.0
GM-MØ specific markers -1.87 0.0
Running Enrichment Score
↑CHIR-Mon
↑DMSO-Mon
Geneset NES FDRq
TOP 200 Genes DOWN ONLY during Mo to GM-MØ 1.48 0.018
TOP 200 Genes DOWN ONLY during Mo to M-MØ -1.46 0.011
TOP 200 Genes UP ONLY during Mo to GM-MØ -1.82 0.0
TOP 200 Genes UP ONLY during Mo to M-MØ 1.64 0.0
E
IL10
CD163
CCL2
Read counts
6.76E-13
2.72E-12
0.063
0.016
6.88E-08
8.43E-22
M-CSF-Mon DMSO-Mon CHIR-Mon
F
Geneset NES FDRq
MAFB dependent genes 1.66 0.0
MAFB inhibited genes -2.56 0.0
G
CHIR-Mon vs. DMSO-Mon
Upregulated CHIR-Mon
733
56
160
M-MØ-specific markers
CCL2 IL10 LGMN CCL8 CD163L1 IGF1 CD28 CD163 MERTK S1PR1
Downregulated CHIR-Mon
1123
129
301
GM-MØ-specific markers
HCAR2 CD1A CD1B CD1C CD1E S100A8 CCR2 APOE CLEC6A
H
CHIR-Mon RASF
CHIR-99021
48 h
Monocytes in RASF
DMSO
DMSO-Mon RASF
I
Monocytes
MAFB
Vinculin
DMSO DMSO CHIR DMSO CHIR DMSO CHIR
RASF #1 RASF #2 RASF #3
MAFB
Normalized densitometry
DMSO-Mon RASF
CHIR-Mon RASF
J
IL10
LGMN
Relative expression
DMSO-Mon RASF
CHIR-Mon RASF

Figure 5

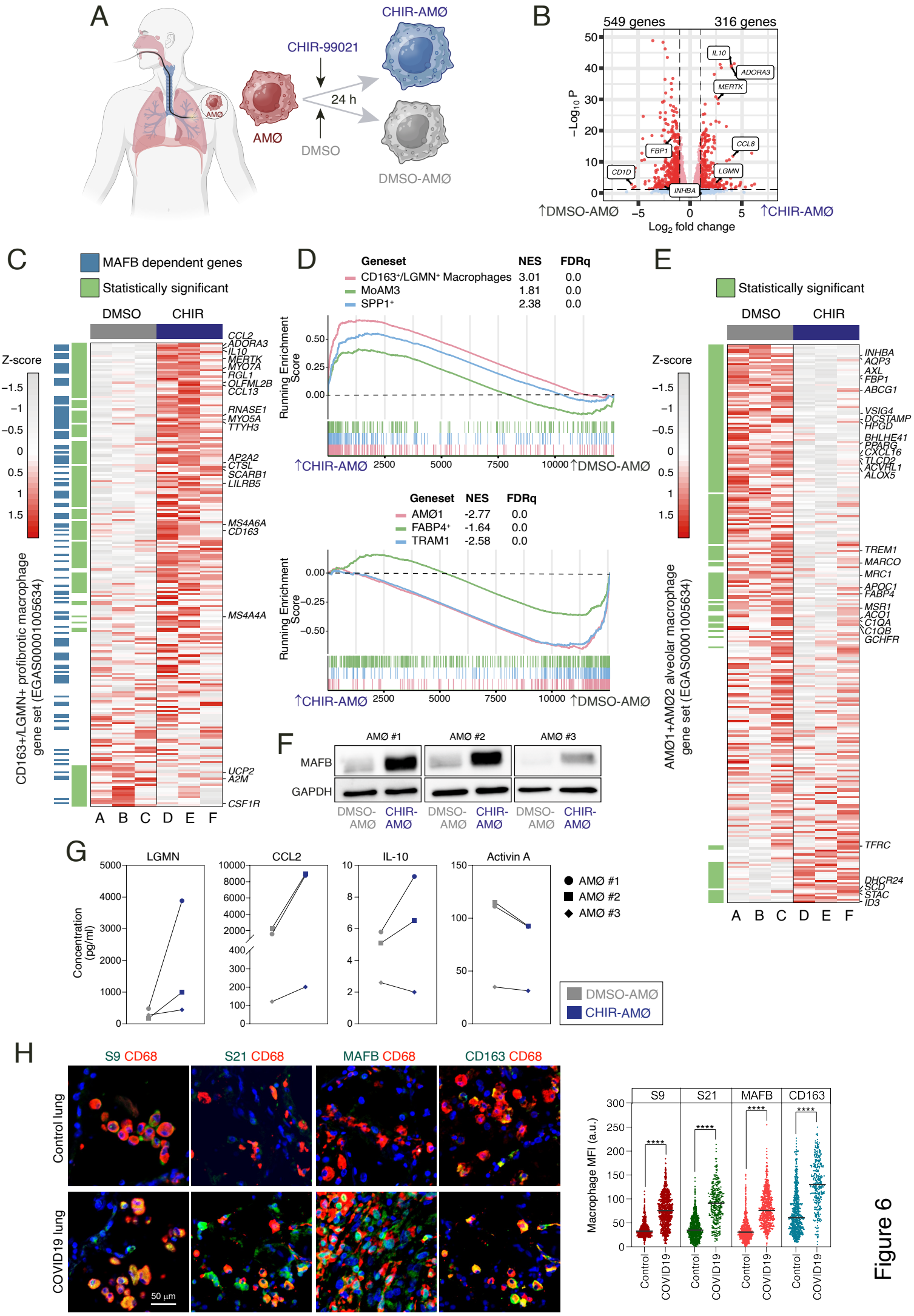
A
CHIR-AMØ
CHIR-99021
24 h
AMØ
DMSO
DMSO-AMØ
B
549 genes
316 genes
IL10
ADORA3
MERTK
CCL8
FBP1
CD1D
LGMN
INHBA
−Log10 P
↑DMSO-AMØ
↑CHIR-AMØ
Log2 fold change
C
MAFB dependent genes
Statistically significant
DMSO
CHIR
Z-score
CCL2
ADORA3
IL10
MERTK
MYO7A
RGL1
OLFML2B
CCL13
RNASE1
MYO5A
TTYH3
AP2A2
CTSL
SCARB1
LILRB5
MS4A6A
CD163
MS4A4A
UCP2
A2M
CSF1R
CD163+/LGMN+ profibrotic macrophage gene set (EGAS00001005634)
A B C D E F
D
Geneset NES FDRq
CD163+/LGMN+ Macrophages 3.01 0.0
MoAM3 1.81 0.0
SPP1+ 2.38 0.0
Running Enrichment Score
↑CHIR-AMØ
↑DMSO-AMØ
Geneset NES FDRq
AMØ1 -2.77 0.0
FABP4+ -1.64 0.0
TRAM1 -2.58 0.0
E
Statistically significant
DMSO
CHIR
Z-score
INHBA
AQP3
AXL
FBP1
ABCG1
VSIG4
DCSTAMP
HPGD
BHLHE41
PPARG
CXCL16
TLCD2
ACVRL1
ALOX5
TREM1
MARCO
MRC1
APOC1
FABP4
MSR1
ACO1
C1QA
C1QB
GCHFR
TFRC
DHCR24
SCD
STAC
ID3
AMØ1+AMØ2 alveolar macrophage gene set (EGAS00001005634)
A B C D E F
F
AMØ #1
AMØ #2
AMØ #3
MAFB
GAPDH
DMSO-AMØ
CHIR-AMØ
G
LGMN
CCL2
IL-10
Activin A
Concentration (pg/ml)
AMØ #1
AMØ #2
AMØ #3
DMSO-AMØ
CHIR-AMØ
H
S9 CD68
S21 CD68
MAFB CD68
CD163 CD68
Control lung
COVID19 lung
50 µm
S9
S21
MAFB
CD163
Macrophage MFI (a.u.)
Control
COVID19
Figure 6

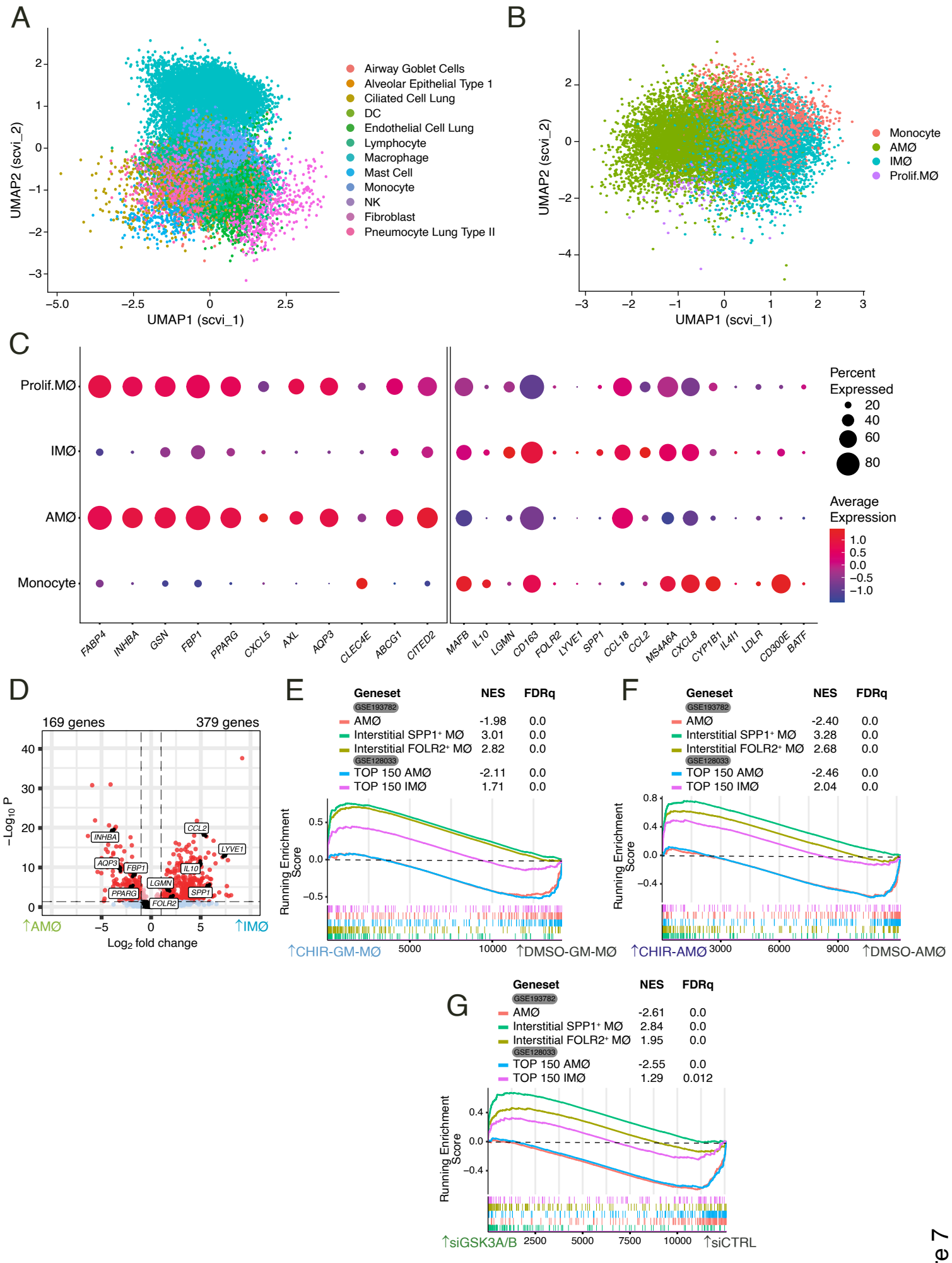
A
UMAP2 (scvi_2)
UMAP1 (scvi_1)
Airway Goblet Cells
Alveolar Epithelial Type 1
Ciliated Cell Lung
DC
Endothelial Cell Lung
Lymphocyte
Macrophage
Mast Cell
Monocyte
NK
Fibroblast
Pneumocyte Lung Type II
B
UMAP2 (scvi_2)
UMAP1 (scvi_1)
Monocyte
AMØ
IMØ
Prolif.MØ
C
Prolif.MØ
IMØ
AMØ
Monocyte
FABP4
INHBA
GSN
FBP1
PPARG
CXCL5
AXL
AQP3
CLEC4E
ABCG1
CITED2
MAFB
IL10
LGMN
CD163
FOLR2
LYVE1
SPP1
CCL18
CCL2
MS4A6A
CXCL8
CYP1B1
IL4I1
LDLR
CD300E
BATF
Percent Expressed
20
40
60
80
Average Expression
1.0
0.5
0.0
−0.5
−1.0
D
169 genes
379 genes
−Log10 P
INHBA
AQP3
FBP1
PPARG
LGMN
FOLR2
CCL2
IL10
SPP1
LYVE1
↑AMØ
↑IMØ
Log2 fold change
E
Geneset
NES
FDRq
GSE193782
AMØ -1.98 0.0
Interstitial SPP1+ MØ 3.01 0.0
Interstitial FOLR2+ MØ 2.82 0.0
GSE128033
TOP 150 AMØ -2.11 0.0
TOP 150 IMØ 1.71 0.0
Running Enrichment Score
↑CHIR-GM-MØ
↑DMSO-GM-MØ
F
Geneset
NES
FDRq
GSE193782
AMØ -2.40 0.0
Interstitial SPP1+ MØ 3.28 0.0
Interstitial FOLR2+ MØ 2.68 0.0
GSE128033
TOP 150 AMØ -2.46 0.0
TOP 150 IMØ 2.04 0.0
Running Enrichment Score
↑CHIR-AMØ
↑DMSO-AMØ
G
Geneset
NES
FDRq
GSE193782
AMØ -2.61 0.0
Interstitial SPP1+ MØ 2.84 0.0
Interstitial FOLR2+ MØ 1.95 0.0
GSE128033
TOP 150 AMØ -2.55 0.0
TOP 150 IMØ 1.29 0.012
Running Enrichment Score
↑siGSK3A/B
↑siCTRL

Figure 7

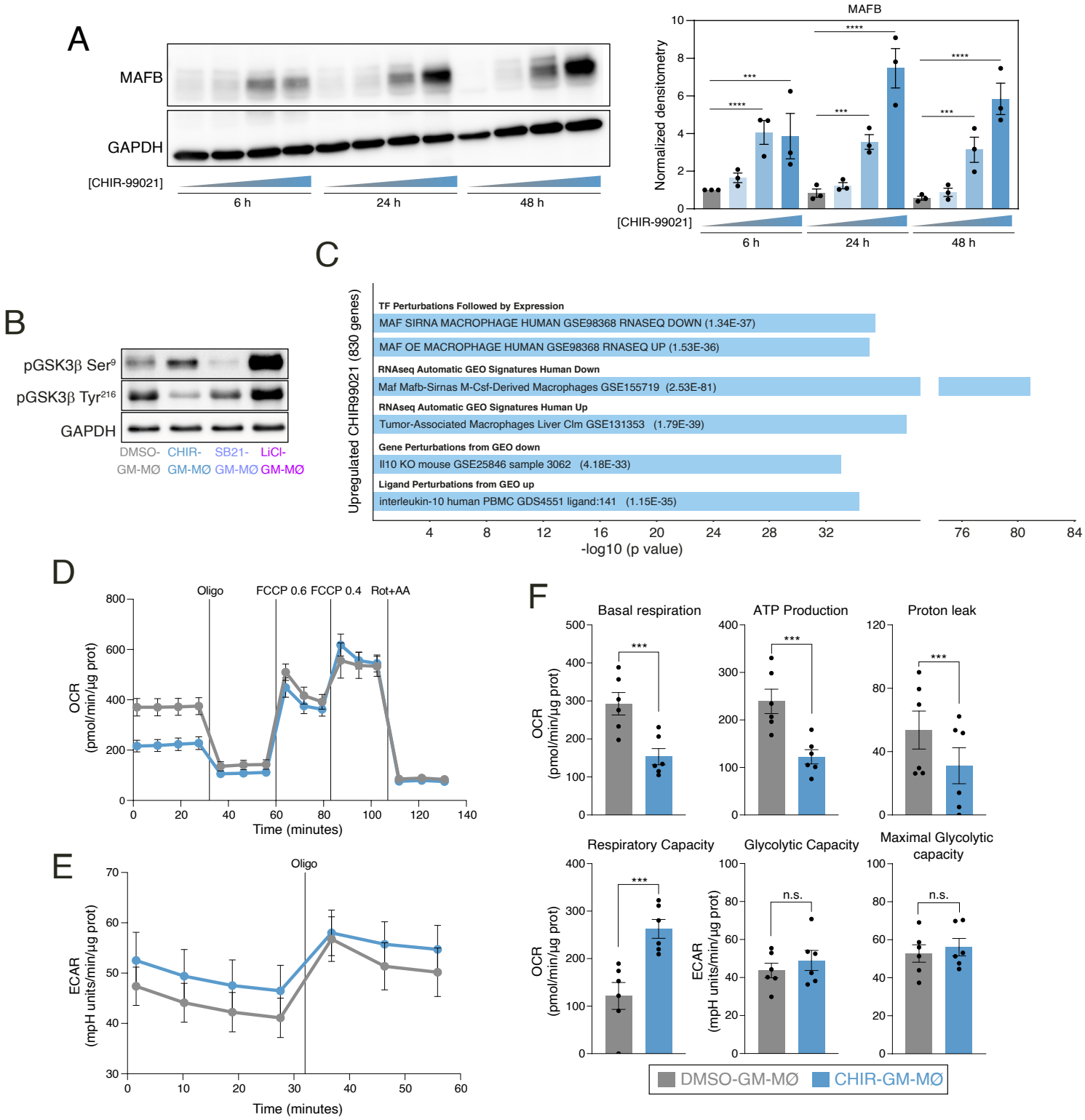
A
MAFB
GAPDH
[CHIR-99021]
6 h
24 h
48 h
MAFB
Normalized densitometry
[CHIR-99021]
6 h
24 h
48 h
B
pGSK3β Ser9
pGSK3β Tyr216
GAPDH
DMSO-GM-MØ
CHIR-GM-MØ
SB21-GM-MØ
LiCl-GM-MØ
C
Upregulated CHIR99021 (830 genes)
TF Perturbations Followed by Expression
MAF SIRNA MACROPHAGE HUMAN GSE98368 RNASEQ DOWN (1.34E-37)
MAF OE MACROPHAGE HUMAN GSE98368 RNASEQ UP (1.53E-36)
RNAseq Automatic GEO Signatures Human Down
Maf Mafb-Sirnas M-Csf-Derived Macrophages GSE155719 (2.53E-81)
RNAseq Automatic GEO Signatures Human Up
Tumor-Associated Macrophages Liver Clm GSE131353 (1.79E-39)
Gene Perturbations from GEO down
Il10 KO mouse GSE25846 sample 3062 (4.18E-33)
Ligand Perturbations from GEO up
interleukin-10 human PBMC GDS4551 ligand:141 (1.15E-35)
-log10 (p value)
D
Oligo
FCCP 0.6
FCCP 0.4
Rot+AA
OCR (pmol/min/µg prot)
Time (minutes)
E
Oligo
ECAR (mpH units/min/µg prot)
Time (minutes)
F
Basal respiration
ATP Production
Proton leak
Respiratory Capacity
Glycolytic Capacity
Maximal Glycolytic capacity
OCR (pmol/min/µg prot)
ECAR (mpH units/min/µg prot)
n.s.
DMSO-GM-MØ
CHIR-GM-MØ

Sup Fig 1

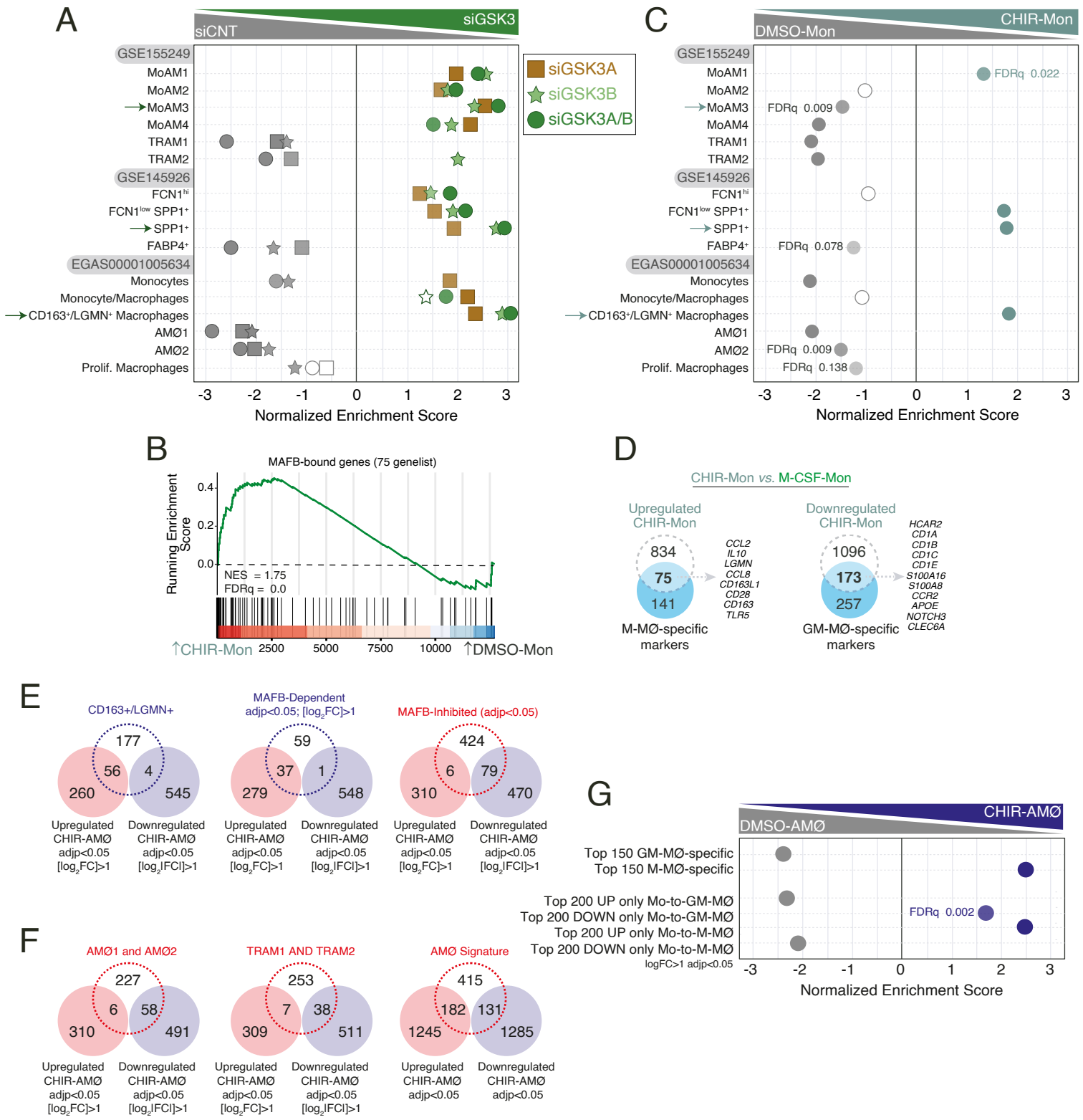
A
siCNT
siGSK3
GSE155249
MoAM1
MoAM2
MoAM3
MoAM4
TRAM1
TRAM2
GSE145926
FCN1hi
FCN1low SPP1+
SPP1+
FABP4+
EGAS00001005634
Monocytes
Monocyte/Macrophages
CD163+/LGMN+ Macrophages
AMØ1
AMØ2
Prolif. Macrophages
siGSK3A
siGSK3B
siGSK3A/B
-3 -2 -1 0 1 2 3
Normalized Enrichment Score
C
DMSO-Mon
CHIR-Mon
FDRq 0.022
FDRq 0.009
FDRq 0.078
FDRq 0.009
FDRq 0.138
Normalized Enrichment Score
B
MAFB-bound genes (75 genelist)
Running Enrichment Score
0.4
0.2
0.0
NES = 1.75
FDRq = 0.0
↑CHIR-Mon 2500 5000 7500 10000 ↑DMSO-Mon
D
CHIR-Mon vs. M-CSF-Mon
Upregulated CHIR-Mon
834
75
141
M-MØ-specific markers
CCL2
IL10
LGMN
CCL8
CD163L1
CD28
CD163
TLR5
Downregulated CHIR-Mon
1096
173
257
GM-MØ-specific markers
HCAR2
CD1A
CD1B
CD1C
CD1E
S100A16
S100A8
CCR2
APOE
NOTCH3
CLEC6A
E
CD163+/LGMN+
177
56
4
260
545
Upregulated CHIR-AMØ adjp<0.05 [log2FC]>1
Downregulated CHIR-AMØ adjp<0.05 [log2|FC|]>1
MAFB-Dependent adjp<0.05; [log2FC]>1
59
37
1
279
548
MAFB-Inhibited (adjp<0.05)
424
6
79
310
470
F
AMØ1 and AMØ2
227
6
58
310
491
TRAM1 AND TRAM2
253
7
38
309
511
AMØ Signature
415
182
131
1245
1285
G
DMSO-AMØ
CHIR-AMØ
Top 150 GM-MØ-specific
Top 150 M-MØ-specific
Top 200 UP only Mo-to-GM-MØ
Top 200 DOWN only Mo-to-GM-MØ
Top 200 UP only Mo-to-M-MØ
Top 200 DOWN only Mo-to-M-MØ
logFC>1 adjp<0.05
FDRq 0.002
Normalized Enrichment Score

Sup Fig 2

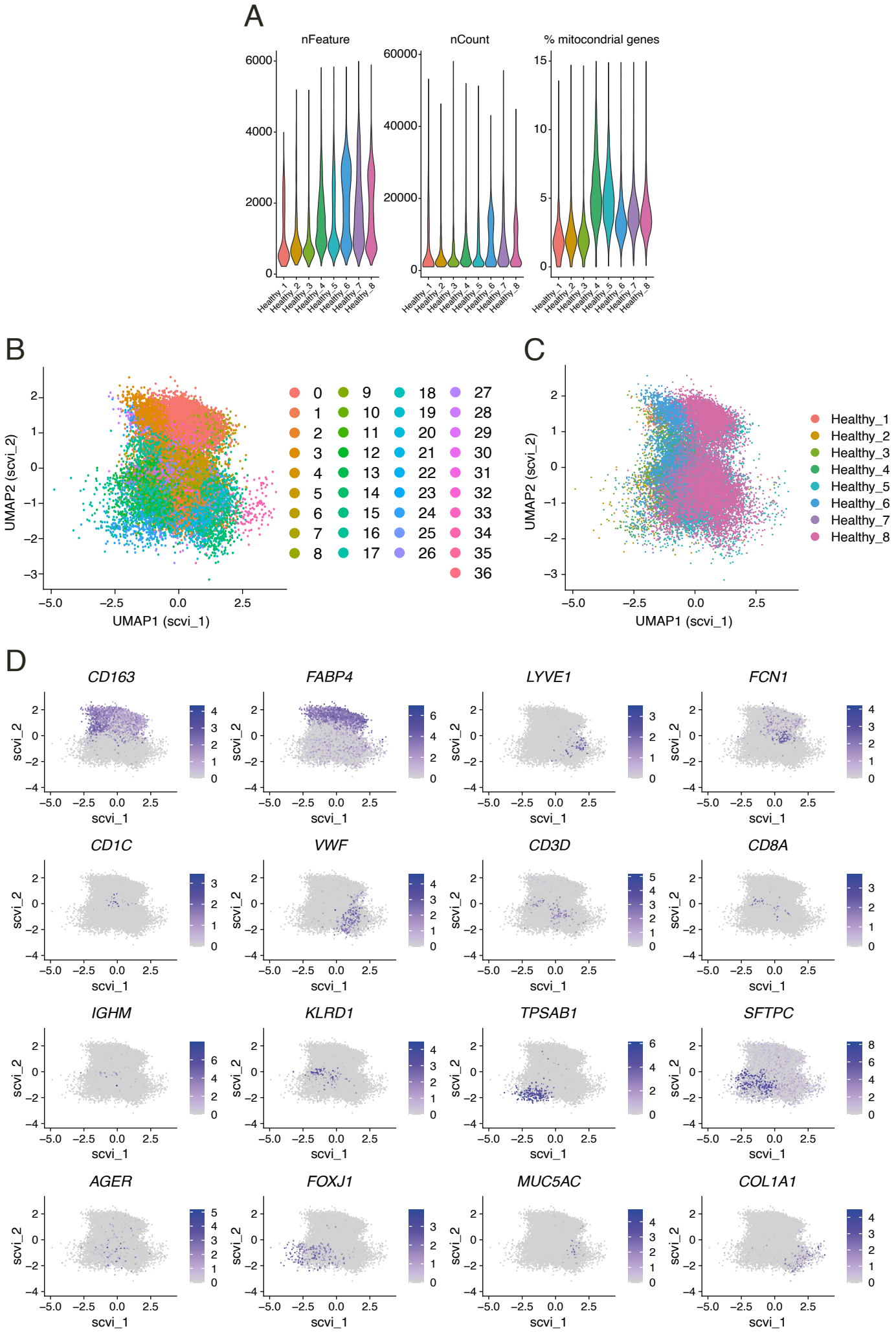
A
nFeature
nCount
% mitocondrial genes
Healthy_1
Healthy_2
Healthy_3
Healthy_4
Healthy_5
Healthy_6
Healthy_7
Healthy_8
B
UMAP2 (scvi_2)
UMAP1 (scvi_1)
C
Healthy_1
Healthy_2
Healthy_3
Healthy_4
Healthy_5
Healthy_6
Healthy_7
Healthy_8
D
CD163
FABP4
LYVE1
FCN1
CD1C
VWF
CD3D
CD8A
IGHM
KLRD1
TPSAB1
SFTPC
AGER
FOXJ1
MUC5AC
COL1A1
scvi_1
scvi_2

Sup Fig 3

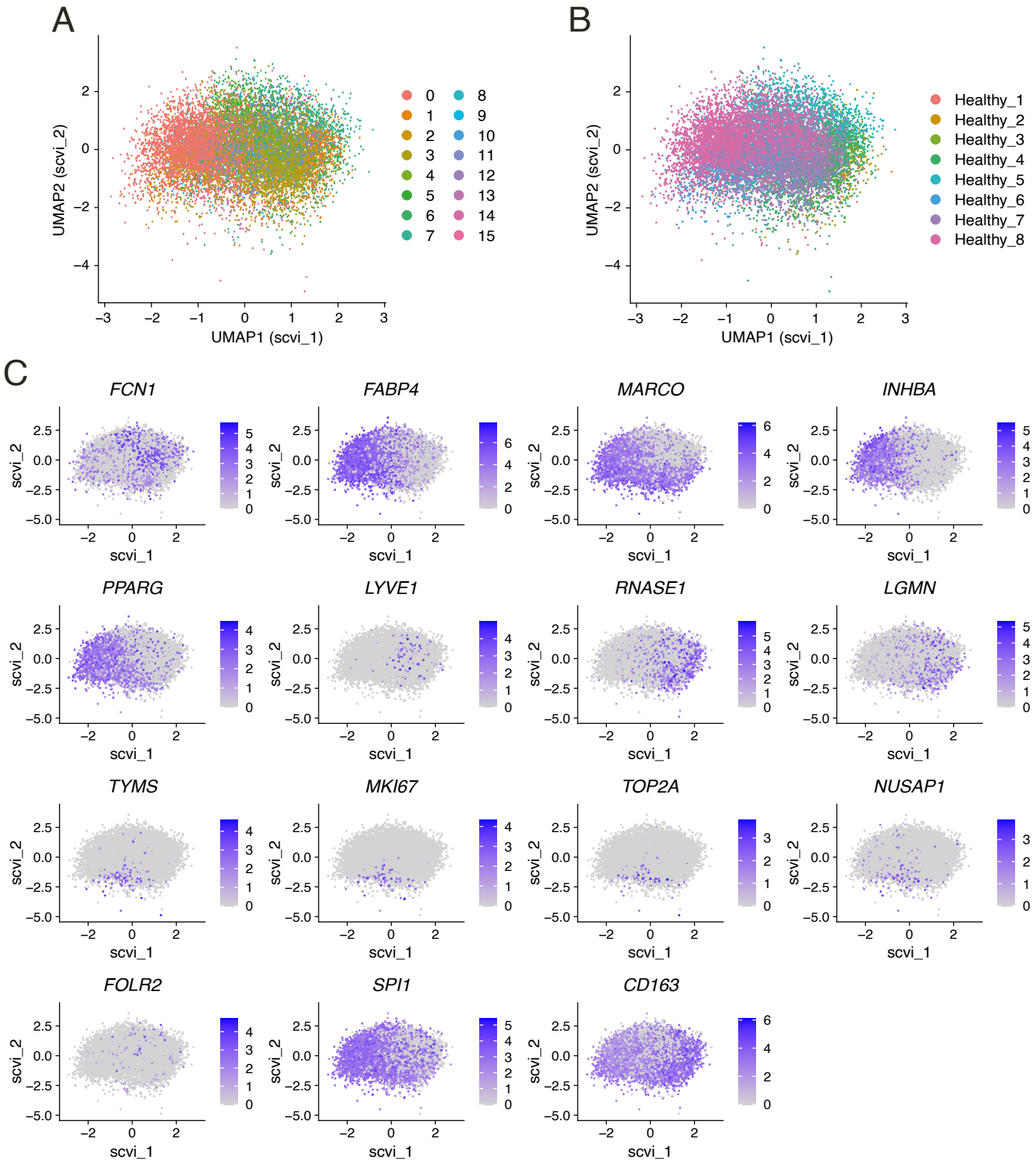
A
UMAP2 (scvi_2)
UMAP1 (scvi_1)
0
1
2
3
4
5
6
7
8
9
10
11
12
13
14
15
B
UMAP2 (scvi_2)
UMAP1 (scvi_1)
Healthy_1
Healthy_2
Healthy_3
Healthy_4
Healthy_5
Healthy_6
Healthy_7
Healthy_8
C
FCN1
FABP4
MARCO
INHBA
PPARG
LYVE1
RNASE1
LGMN
TYMS
MKI67
TOP2A
NUSAP1
FOLR2
SPI1
CD163
scvi_1
scvi_2

Sup Fig 4

Supplementary Table 1.

Transcriptional datasets used in the present study

| Reference | Gene set at Baseline: RNA-Seq, 2021 | | | | | | Gene set at 1 year: RNA-Seq, 2021 | | | | | | Microbiota at at D21 (GR-ASAP, 2020) | | | | | | Genotype data at the Ghilge and Freed lymphoid CUBE/GEN, 2021; Mellor et al. Int J Med Sci 24-2021, 2020 | | | | | | Genotype data at the Ghilge and Freed lymphoid CUBE/GEN, 2021; Mellor et al. Int J Med Sci 24-2021, 2020 | | | | | | Mellor et al Immunity 53:1493-1506, 2021 | | | | | |

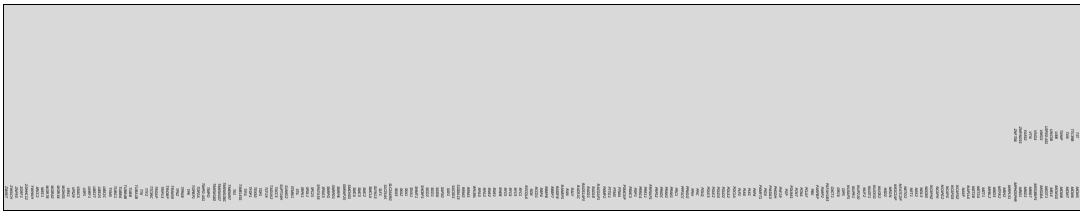

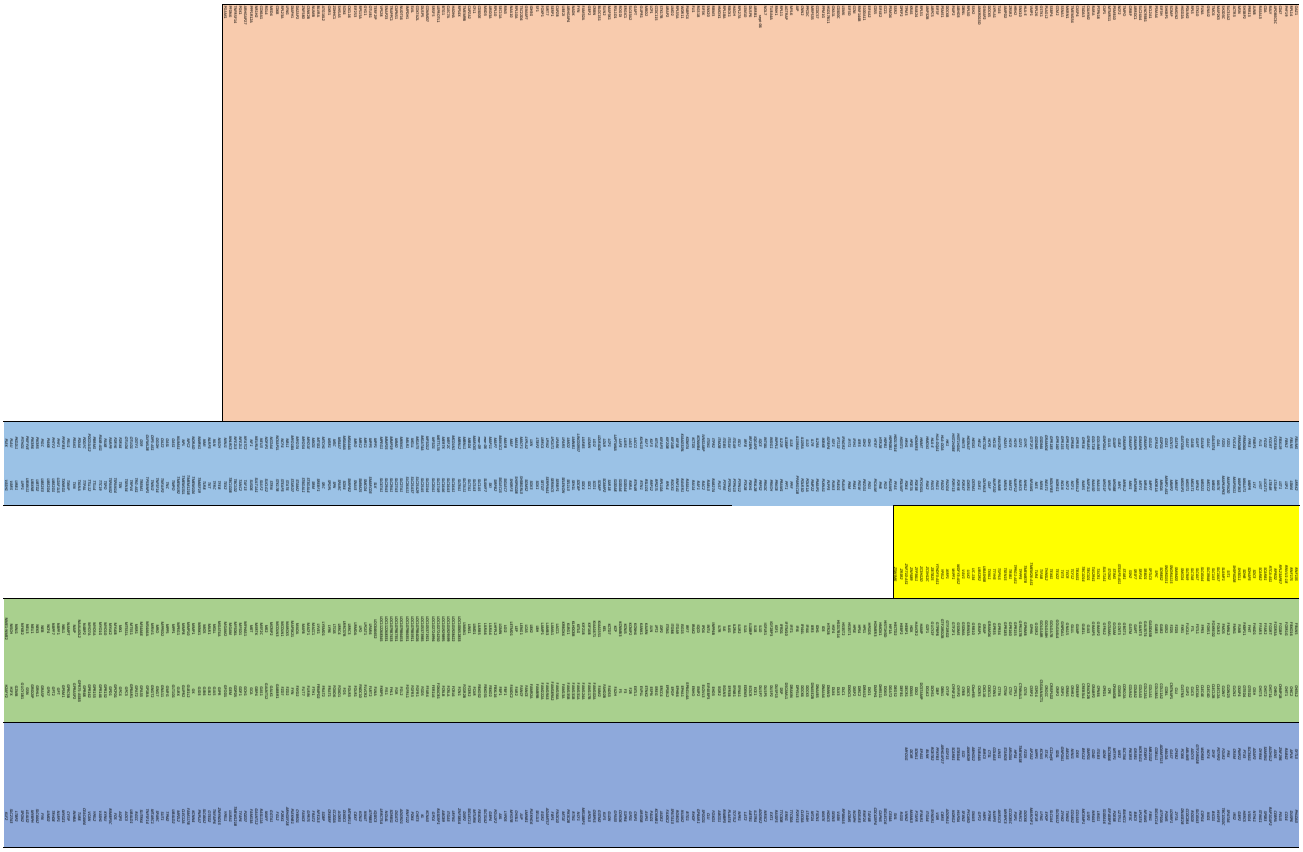

PLD1B2	UGT
PLD1B3	VCAN
PLD2	VCL
PLD3	VDR
PLK1S1	VEGFA
POF	VEK
PPA1X	VHL1B
PPCS	WASF2
PPFIBP1	WDR1
PPFIA1L1	YAP1
PPFIA3	ZC3H12D
PPFIBP2	ZFAND5
PPL1A2	ZFAN1B
PQCN4	ZFYVE16
PRC1L	ZNED1-AS1
PRCP	ZNF138
PRDM1	ZNF185
PRF1L	ZNF540
PRL1B2	ZNF697
PRL1B3	ZNF804A
PTC1A2	
PTC1B2	
PTCH1B4	
PTC2B	
PTCH1	
PTPN11	
PTPN4	
PTPN6	
PTX1	
QKI	
RAB11	
RAB14L2	
RAB1C	
RAB 1B	
RAB4A	
RAB5A	
RAB7B	
RAB1A2	
RAC1	
RAC1B1	
RAC1B2	
RAC1B3	
RAF	
RAGA2	
RAGD	
RAI1	
RAI14	
RAI14	
RAP1A	
RAP1B	
RAP2A	
RAP2B	
RAP2C	
RAP1	
RAP1A	
RAP1B	
RAP2	
RAPGEF1	
RAPGEF2	
RAPGEF3	
RAPGEF4	
RAPGEF5	
RAPGEF6	
RAPH1	
RAPH2	
RAPH3	
RAPH4	
RAPH5	
RAPH6	
RAPH7	
RAPH8	
RAPH9	
RAPH10	
RAPH11	
RAPH12	
RAPH13	
RAPH14	
RAPH15	
RAPH16	
RAPH17	
RAPH18	
RAPH19	
RAPH20	
RAPH21	
RAPH22	
RAPH23	
RAPH24	
RAPH25	
RAPH26	
RAPH27	
RAPH28	
RAPH29	
RAPH30	
RAPH31	
RAPH32	
RAPH33	
RAPH34	
RAPH35	
RAPH36	
RAPH37	
RAPH38	
RAPH39	
RAPH40	
RAPH41	
RAPH42	
RAPH43	
RAPH44	
RAPH45	
RAPH46	
RAPH47	
RAPH48	
RAPH49	
RAPH50	
RAPH51	
RAPH52	
RAPH53	
RAPH54	
RAPH55	
RAPH56	
RAPH57	
RAPH58	
RAPH59	
RAPH60	
RAPH61	
RAPH62	
RAPH63	
RAPH64	
RAPH65	
RAPH66	
RAPH67	
RAPH68	
RAPH69	
RAPH70	
RAPH71	
RAPH72	
RAPH73	
RAPH74	
RAPH75	
RAPH76	
RAPH77	
RAPH78	
RAPH79	
RAPH80	
RAPH81	
RAPH82	
RAPH83	
RAPH84	
RAPH85	
RAPH86	
RAPH87	
RAPH88	
RAPH89	
RAPH90	
RAPH91	
RAPH92	
RAPH93	
RAPH94	
RAPH95	
RAPH96	
RAPH97	
RAPH98	
RAPH99	
RAPH100	
RAPH101	
RAPH102	
RAPH103	
RAPH104	
RAPH105	
RAPH106	
RAPH107	
RAPH108	
RAPH109	
RAPH110	
RAPH111	
RAPH112	
RAPH113	
RAPH114	
RAPH115	
RAPH116	
RAPH117	
RAPH118	
RAPH119	
RAPH120	
RAPH121	
RAPH122	
RAPH123	
RAPH124	
RAPH125	
RAPH126	
RAPH127	
RAPH128	
RAPH129	
RAPH130	
RAPH131	
RAPH132	
RAPH133	
RAPH134	
RAPH135	
RAPH136	
RAPH137	
RAPH138	
RAPH139	
RAPH140	
RAPH141	
RAPH142	
RAPH143	
RAPH144	
RAPH145	
RAPH146	
RAPH147	
RAPH148	
RAPH149	
RAPH150	
RAPH151	
RAPH152	
RAPH153	
RAPH154	
RAPH155	
RAPH156	
RAPH157	
RAPH158	
RAPH159	
RAPH160	
RAPH161	
RAPH162	
RAPH163	
RAPH164	
RAPH165	
RAPH166	
RAPH167	
RAPH168	
RAPH169	
RAPH170	
RAPH171	
RAPH172	
RAPH173	
RAPH174	
RAPH175	
RAPH176	
RAPH177	
RAPH178	
RAPH179	
RAPH180	
RAPH181	
RAPH182	
RAPH183	
RAPH184	
RAPH185	
RAPH186	
RAPH187	
RAPH188	
RAPH189	
RAPH190	
RAPH191	
RAPH192	
RAPH193	
RAPH194	
RAPH195	
RAPH196	
RAPH197	
RAPH198	
RAPH199	
RAPH200	
RAPH201	
RAPH202	
RAPH203	
RAPH204	
RAPH205	
RAPH206	
RAPH207	
RAPH208	
RAPH209	
RAPH210	
RAPH211	
RAPH212	
RAPH213	
RAPH214	
RAPH215	
RAPH216	
RAPH217	
RAPH218	
RAPH219	
RAPH220	
RAPH221	
RAPH222	
RAPH223	
RAPH224	
RAPH225	
RAPH226	
RAPH227	
RAPH228	
RAPH229	
RAPH230	
RAPH231	
RAPH232	
RAPH233	
RAPH234	
RAPH235	
RAPH236	
RAPH237	
RAPH238	
RAPH239	
RAPH240	
RAPH241	
RAPH242	
RAPH243	
RAPH244	
RAPH245	
RAPH246	
RAPH247	
RAPH248	
RAPH249	
RAPH250	
RAPH251	
RAPH252	
RAPH253	
RAPH254	
RAPH255	
RAPH256	
RAPH257	
RAPH258	
RAPH259	
RAPH260	
RAPH261	
RAPH262	
RAPH263	
RAPH264	
RAPH265	
RAPH266	
RAPH267	
RAPH268	
RAPH269	
RAPH270	
RAPH271	
RAPH272	
RAPH273	
RAPH274	
RAPH275	
RAPH276	
RAPH277	
RAPH278	
RAPH279	
RAPH280	
RAPH281	
RAPH282	
RAPH283	
RAPH284	
RAPH285	
RAPH286	
RAPH287	
RAPH288	
RAPH289	
RAPH290	
RAPH291	
RAPH292	
RAPH293	
RAPH294	
RAPH295	
RAPH296	
RAPH297	
RAPH298	
RAPH299	
RAPH300	
RAPH301	
RAPH302	
RAPH303	
RAPH304	
RAPH305	
RAPH306	
RAPH307	
RAPH308	
RAPH309	
RAPH310	
RAPH311	
RAPH312	
RAPH313	
RAPH314	
RAPH315	
RAPH316	
RAPH317	
RAPH318	
RAPH319	
RAPH320	
RAPH321	
RAPH322	
RAPH323	
RAPH324	
RAPH325	
RAPH326	
RAPH327	
RAPH328	
RAPH329	
RAPH330	
RAPH331	
RAPH332	
RAPH333	
RAPH334	
RAPH335	
RAPH336	
RAPH337	
RAPH338	
RAPH339	
RAPH340	
RAPH341	
RAPH342	
RAPH343	
RAPH344	
RAPH345	
RAPH346	
RAPH347	
RAPH348	
RAPH349	
RAPH350	
RAPH351	
RAPH352	
RAPH353	
RAPH354	
RAPH355	
RAPH356	
RAPH357	
RAPH358	
RAPH359	
RAPH360	
RAPH361	
RAPH362	
RAPH363	
RAPH364	
RAPH365	
RAPH366	
RAPH367	
RAPH368	
RAPH369	
RAPH370	
RAPH371	
RAPH372	
RAPH373	
RAPH374	
RAPH375	
RAPH376	
RAPH377	
RAPH378	
RAPH379	
RAPH380	
RAPH381	
RAPH382	
RAPH383	
RAPH384	
RAPH385	
RAPH386	
RAPH387	
RAPH388	
RAPH389	
RAPH390	
RAPH391	
RAPH392	
RAPH393	
RAPH394	
RAPH395	
RAPH396	
RAPH397	
RAPH398	
RAPH399	
RAPH400	
RAPH401	
RAPH402	
RAPH403	
RAPH404	
RAPH405	
RAPH406	
RAPH407	
RAPH408	
RAPH409	
RAPH410	
RAPH411	
RAPH412	
RAPH413	
RAPH414	
RAPH415	
RAPH416	
RAPH417	
RAPH418	
RAPH419	
RAPH420	
RAPH421	
RAPH422	
RAPH423	
RAPH424	
RAPH425	
RAPH426	
RAPH427	
RAPH428	
RAPH429	
RAPH430	
RAPH431	
RAPH432	
RAPH433	
RAPH434	
RAPH435	
RAPH436	
RAPH437	
RAPH438	
RAPH439	
RAPH440	
RAPH441	
RAPH442	
RAPH443	
RAPH444	
RAPH445	
RAPH446	
RAPH447	
RAPH448	
RAPH449	
RAPH450	
RAPH451	
RAPH452	
RAPH453	
RAPH454	
RAPH455	
RAPH456	
RAPH457	
RAPH458	
RAPH459	
RAPH460	
RAPH461	
RAPH462	
RAPH463	
RAPH464	
RAPH465	
RAPH466	
RAPH467	
RAPH468	
RAPH469	
RAPH470	
RAPH471	
RAPH472	
RAPH473	
RAPH474	
RAPH475	
RAPH476	
RAPH477	
RAPH478	
RAPH479	
RAPH480	
RAPH481	
RAPH482	
RAPH483	
RAPH484	
RAPH485	
RAPH486	
RAPH487	
RAPH488	
RAPH489	
RAPH490	
RAPH491	
RAPH492	
RAPH493	
RAPH494	
RAPH495	
RAPH496	
RAPH497	
RAPH498	
RAPH499	
RAPH500	
RAPH501	
RAPH502	
RAPH503	
RAPH504	
RAPH505	
RAPH506	
RAPH507	
RAPH508	
RAPH509	
RAPH510	
RAPH511	
RAPH512	
RAPH513	
RAPH514	
RAPH515	
RAPH516	
RAPH517	
RAPH518	
RAPH519	
RAPH520	
RAPH521	
RAPH522	
RAPH523	
RAPH524	
RAPH525	
RAPH526	
RAPH527	
RAPH528	
RAPH529	
RAPH530	
RAPH531	
RAPH532	
RAPH533	
RAPH534	
RAPH535	
RAPH536	
RAPH537	
RAPH538	
RAPH539	
RAPH540	
RAPH541	
RAPH542	
RAPH543	
RAPH544	
RAPH545	
RAPH546	
RAPH547	
RAPH548	
RAPH549	
RAPH550	
RAPH551	
RAPH552	
RAPH553	
RAPH554	
RAPH555	
RAPH556	
RAPH557	
RAPH558	
RAPH559	
RAPH560	
RAPH561	
RAPH562	
RAPH563	
RAPH564	
RAPH565	
RAPH566	
RAPH567	
RAPH568	
RAPH569	
RAPH570	
RAPH571	
RAPH572	
RAPH573	
RAPH574	
RAPH575	
RAPH576	
RAPH577	
RAPH578	
RAPH579	
RAPH580	
RAPH581	
RAPH582	
RAPH583	
RAPH584	
RAPH585	
RAPH586	
RAPH587	
RAPH588	
RAPH589	
RAPH590	
RAPH591	
RAPH592	
RAPH593	
RAPH594	
RAPH595	
RAPH596	
RAPH597	
RAPH598	
RAPH599	
RAPH600	
RAPH601	
RAPH602	
RAPH603	
RAPH604	
RAPH605	
RAPH606	
RAPH607	
RAPH608	
RAPH609	
RAPH610	
RAPH611	
RAPH612	
RAPH613	
RAPH614	
RAPH615	
RAPH616	
RAPH617	
RAPH618	
RAPH619	
RAPH620	
RAPH621	
RAPH622	
RAPH623	
RAPH624	
RAPH625	
RAPH626	
RAPH627	
RAPH628	
RAPH629	
RAPH630	
RAPH631	
RAPH632	
RAPH633	
RAPH634	
RAPH635	
RAPH636	
RAPH637	
RAPH638	
RAPH639	
RAPH640	
RAPH641	
RAPH642	
RAPH643	
RAPH644	
RAPH645	
RAPH646	
RAPH647	
RAPH648	
RAPH649	
RAPH650	
RAPH651	
RAPH652	
RAPH653	
RAPH654	
RAPH655	
RAPH656	
RAPH657	
RAPH658	
RAPH659	
RAPH660	
RAPH661	
RAPH662	
RAPH663	
RAPH664	
RAPH665	
RAPH666	
RAPH667	
RAPH668	
RAPH669	
RAPH670	
RAPH671	
RAPH672	
RAPH673	
RAPH674	
RAPH675	
RAPH676	
RAPH677	
RAPH678	
RAPH679	
RAPH680	
RAPH681	
RAPH682	
RAPH683	
RAPH684	
RAPH685	
RAPH686	
RAPH687	
RAPH688	
RAPH689	
RAPH690	
RAPH691	
RAPH692	
RAPH693	
RAPH694	
RAPH695	
RAPH696	
RAPH697	
RAPH698	
RAPH699	
RAPH700	
RAPH701	
RAPH702	
RAPH703	
RAPH704	
RAPH705	
RAPH706	
RAPH707	
RAPH708	
RAPH709	
RAPH710	
RAPH711	
RAPH712	
RAPH713	
RAPH714	
RAPH715	
RAPH716	
RAPH717	
RAPH718	
RAPH719	
RAPH720	
RAPH721	
RAPH722	
RAPH723	
RAPH724	
RAPH725	
RAPH726	
RAPH727	
RAPH728	
RAPH729	
RAPH730	
RAPH731	
RAPH732	
RAPH733	
RAPH734	
RAPH735	
RAPH736	
RAPH737	
RAPH738	
RAPH739	
RAPH740	
RAPH741	
RAPH742	
RAPH743	
RAPH744	
RAPH745	
RAPH746	
RAPH747	
RAPH748	
RAPH749	
RAPH750	
RAPH751	
RAPH752	
RAPH753	
RAPH754	
RAPH755	
RAPH756	
RAPH757	
RAPH758	
RAPH759	
RAPH760	
RAPH761	
RAPH762	
RAPH763	
RAPH764	
RAPH765	
RAPH766	
RAPH767	
RAPH768	
RAPH769	
RAPH770	
RAPH771	
RAPH772	
RAPH773	
RAPH774	
RAPH775	
RAPH776	
RAPH777	
RAPH778	
RAPH779	
RAPH780	
RAPH781	
RAPH782	
RAPH783	
RAPH784	
RAPH785	
RAPH786	
RAPH787	
RAPH788	
RAPH789	
RAPH790	
RAPH791	
RAPH792	
RAPH793	
RAPH794	
RAPH795	
RAPH796	
RAPH797	
RAPH798	
RAPH799	
RAPH800	
RAPH801	
RAPH802	
RAPH803	
RAPH804	
RAPH805	
RAPH806	
RAPH807	
RAPH808	
RAPH809	
RAPH810	
RAPH811	
RAPH812	
RAPH813	
RAPH814	
RAPH815	
RAPH816	
RAPH817	
RAPH818	
RAPH819	
RAPH820	
RAPH821	
RAPH822	
RAPH823	
RAPH824	
RAPH825	
RAPH826	
RAPH827	
RAPH828	
RAPH829	
RAPH830	
RAPH831	
RAPH832	
RAPH833	
RAPH834	
RAPH835	
RAPH836	
RAPH837	
RAPH838	
RAPH839	
RAPH840	
RAPH841	
RAPH842	
RAPH843	
RAPH844	
RAPH845	
RAPH846	
RAPH847	
RAPH848	
RAPH849	
RAPH850	
RAPH851	
RAPH852	
RAPH853	
RAPH854	
RAPH855	
RAPH856	
RAPH857	
RAPH858	
RAPH859	
RAPH860	
RAPH861	
RAPH862	
RAPH863	
RAPH864	
RAPH865	
RAPH866	
RAPH867	
RAPH868	
RAPH869	
RAPH870	
RAPH871	
RAPH872	
RAPH873	
RAPH874	
RAPH875	
RAPH876	
RAPH877	
RAPH878	
RAPH879	
RAPH880	
RAPH881	
RAPH882	
RAPH883	
RAPH884	
RAPH885	
RAPH886	
RAPH887	
RAPH888	
RAPH889	
RAPH890	
RAPH891	
RAPH892	
RAPH893	
RAPH894	
RAPH895	
RAPH896	
RAPH897	
RAPH898	
RAPH899	
RAPH900	
RAPH901	
RAPH902	
RAPH903	
RAPH904	
RAPH905	
RAPH906	
RAPH907	
RAPH908	
RAPH909	
RAPH910	
RAPH911	
RAPH912	
RAPH913	
RAPH914	
RAPH915	
RAPH916	
RAPH917	
RAPH918	
RAPH919	
RAPH920	
RAPH921	
RAPH922	
RAPH923	
RAPH924	
RAPH925	
RAPH926	
RAPH927	
RAPH928	
RAPH929	
RAPH930	
RAPH931	
RAPH932	
RAPH933	
RAPH934	
RAPH935	
RAPH936	
RAPH937	
RAPH938	
RAPH939	
RAPH940	
RAPH941	
RAPH942	
RAPH943	
RAPH944	
RAPH945	
RAPH946	
RAPH947	
RAPH948	
RAPH949	
RAPH950	
RAPH951	
RAPH952	
RAPH953	
RAPH954	
RAPH955	
RAPH956	
RAPH957	
RAPH958	
RAPH959	
RAPH960	
RAPH961	
RAPH962	
RAPH963	
RAPH964	
RAPH965	
RAPH966	
RAPH967	
RAPH968	
RAPH969	
RAPH970	
RAPH971	
RAPH972	
RAPH973	
RAPH974	
RAPH975	
RAPH976	
RAPH977	
RAPH978	
RAPH979	
RAPH980	
RAPH981	
RAPH982	
RAPH983	
RAPH984	
RAPH985	
RAPH986	
RAPH987	
RAPH988	
RAPH989	
RAPH990	
RAPH991	
RAPH992	
RAPH993	
RAPH994	
RAPH995	
RAPH996	
RAPH997	
RAPH998	
RAPH999	
RAPH1000	

3M2
AAUR14
6BF52
6BF53
6GPY2
6GPY3
6GRY2
3HPT2
6GRY3
6GPY2
JR07
JR08
ZGN1B
ZGN4Z
ZFYN1J
ZFYCE
ZNF2B
ZNA2
ZNG1AM
ZNF10
ZNF102
ZNF398
ZNF395
ZNF396
ZNF397
ZNF397
ZNF398
ZNF398
ZGN3B
ZGN4B
ZZY1

TMRA21B	MRV47
TMRA8A01	MYF6
TMRA20B	MYBPC3
TMRA21B	MYH7
TMRA21B	MYH7
TMRA20B	MYOM
TMRA20B	MYOMP
TMRA21B	MYO
TMRA21B	NAP1L2
TMRA21B	NBN7B
TMRA21B	NBN7B
TMRA21B	NCAM1
TMRA21B	NDUFA1
TMRA21B	NDUFA1
TMRA21B	NDUFA

S100A10
S100A16
S100A3
S100A4
S100A6
S1PR1
S1PR2
SAA2
SAA4
SAT1
SCF
SCN5A
SDC1
SEC14L2
SEC61G
SERPINA1
SFN
SFRP1
SFRP2
SFRP4
SGK1
SGMS1
SGMS2
SGPP1
SGPP2
SH2B3
SH3BP4
SH3BP5
SH3GL3
SHANK2
SHC1
SHD
SHE
SHF
SHISA2
SHISA3
SHISA5
SHMT2
SHOC2
SHPRH
SHPRH2DA
SIAE
SIAH2
SIAH2AS1
SIGIRR
SIGLEC11
SIGLEC14
SIGLEC15
SIGLEC16
SIK3
SIL1
SLC1A3
SLC1A4
SLC1A5
SLC1A7
SLC2A1
SLC2A3
SLC2A4
SLC2A5
SLC2A6
SLC2A8
SLC2A9
SLC2A10
SLC2A11
SLC2A12
SLC2A13
SLC2A14
SLC2A15
SLC2A1AS
SLC2A2
SLC2A3AS
SLC2A4AS
SLC2A5AS
SLC2A6AS
SLC2A8AS
SLC2A9AS
SLC3A2
SLC3A6
SLC4A1
SLC4A2
SLC4A3
SLC4A4
SLC4A5
SLC4A7
SLC4A8
SLC4A9
SLC5A1
SLC5A2
SLC5A3
SLC5A4
SLC5A5
SLC5A6
SLC5A7
SLC5A8
SLC5A9
SLC6A1
SLC6A2
SLC6A3
SLC6A4
SLC6A5
SLC6A6
SLC6A7
SLC6A8
SLC6A9
SLC6A11
SLC6A12
SLC6A13
SLC6A14
SLC6A15
SLC6A16
SLC6A17
SLC6A18
SLC7A1
SLC7A2
SLC7A3
SLC7A4
SLC7A5
SLC7A6
SLC7A7
SLC7A8
SLC7A9
SLC7A10
SLC7A11
SLC7A13
SLC7A14
SLC8A1
SLC8A2
SLC8A3
SLC9A1
SLC9A2
SLC9A3
SLC9A4
SLC9A5
SLC9A6
SLC9A7
SLC9A8
SLC9A9
SLC9A10
SLC9A11
SLC9A1AS
SLC9A2AS
SLC9A3AS
SLC9A4AS
SLC9A5AS
SLC9A6AS
SLC9A7AS
SLC9A8AS
SLC9A9AS
SLC9A10AS
SLC9A11AS
SLC9B2
SLC9C1
SLC9C2
SLC9C3
SLC9C4
SLC9C5
SLC9C6
SLC9C7
SLC9C8
SLC9C9
SLC9C10
SLC9C11
SLC9C12
SLC9C13
SLC9C14
SLC9C15
SLC9C16
SLC9C17
SLC9C18
SLC9C19
SLC9C20
SLC9C21
SLC9C22
SLC9C23
SLC9C24
SLC9C25
SLC9C26
SLC9C27
SLC9C28
SLC9C29
SLC9C30
SLC9C31
SLC9C32
SLC9C33
SLC9C34
SLC9C35
SLC9C36
SLC9C37
SLC9C38
SLC9C39
SLC9C40
SLC9C41
SLC9C42
SLC9C43
SLC9C44
SLC9C45
SLC9C46
SLC9C47
SLC9C48
SLC9C49
SLC9C50
SLC9C51
SLC9C52
SLC9C53
SLC9C54
SLC9C55
SLC9C56
SLC9C57
SLC9C58
SLC9C59
SLC9C60
SLC9C61
SLC9C62
SLC9C63
SLC9C64
SLC9C65
SLC9C66
SLC9C67
SLC9C68
SLC9C69
SLC9C70
SLC9C71
SLC9C72
SLC9C73
SLC9C74
SLC9C75
SLC9C76
SLC9C77
SLC9C78
SLC9C79
SLC9C80
SLC9C81
SLC9C82
SLC9C83
SLC9C84
SLC9C85
SLC9C86
SLC9C87
SLC9C88
SLC9C89
SLC9C90
SLC9C91
SLC9C92
SLC9C93
SLC9C94
SLC9C95
SLC9C96
SLC9C97
SLC9C98
SLC9C99
SLC9C100
SLC9C101
SLC9C102
SLC9C103
SLC9C104
SLC9C105
SLC9C106
SLC9C107
SLC9C108
SLC9C109
SLC9C110
SLC9C111
SLC9C112
SLC9C113
SLC9C114
SLC9C115
SLC9C116
SLC9C117
SLC9C118
SLC9C119
SLC9C120
SLC9C121
SLC9C122
SLC9C123
SLC9C124
SLC9C125
SLC9C126
SLC9C127
SLC9C128
SLC9C129
SLC9C130
SLC9C131
SLC9C132
SLC9C133
SLC9C134
SLC9C135
SLC9C136
SLC9C137
SLC9C138
SLC9C139
SLC9C140
SLC9C141
SLC9C142
SLC9C143
SLC9C144
SLC9C145
SLC9C146
SLC9C147
SLC9C148
SLC9C149
SLC9C150
SLC9C151
SLC9C152
SLC9C153
SLC9C154
SLC9C155
SLC9C156
SLC9C157
SLC9C158
SLC9C159
SLC9C160
SLC9C161
SLC9C162
SLC9C163
SLC9C164
SLC9C165
SLC9C166
SLC9C167
SLC9C168
SLC9C169
SLC9C170
SLC9C171
SLC9C172
SLC9C173
SLC9C174
SLC9C175
SLC9C176
SLC9C177
SLC9C178
SLC9C179
SLC9C180
SLC9C181
SLC9C182
SLC9C183
SLC9C184
SLC9C185
SLC9C186
SLC9C187
SLC9C188
SLC9C189
SLC9C190
SLC9C191
SLC9C192
SLC9C193
SLC9C194
SLC9C195
SLC9C196
SLC9C197
SLC9C198
SLC9C199
SLC9C200
SLC9C201
SLC9C202
SLC9C203
SLC9C204
SLC9C205
SLC9C206
SLC9C207
SLC9C208
SLC9C209
SLC9C210
SLC9C211
SLC9C212
SLC9C213
SLC9C214
SLC9C215
SLC9C216
SLC9C217
SLC9C218
SLC9C219
SLC9C220
SLC9C221
SLC9C222
SLC9C223
SLC9C224
SLC9C225
SLC9C226
SLC9C227
SLC9C228
SLC9C229
SLC9C230
SLC9C231
SLC9C232
SLC9C233
SLC9C234
SLC9C235
SLC9C236
SLC9C237
SLC9C238
SLC9C239
SLC9C240
SLC9C241
SLC9C242
SLC9C243
SLC9C244
SLC9C245
SLC9C246
SLC9C247
SLC9C248
SLC9C249
SLC9C250
SLC9C251
SLC9C252
SLC9C253
SLC9C254
SLC9C255
SLC9C256
SLC9C257
SLC9C258
SLC9C259
SLC9C260
SLC9C261
SLC9C262
SLC9C263
SLC9C264
SLC9C265
SLC9C266
SLC9C267
SLC9C268
SLC9C269
SLC9C270
SLC9C271
SLC9C272
SLC9C273
SLC9C274
SLC9C275
SLC9C276
SLC9C277
SLC9C278
SLC9C279
SLC9C280
SLC9C281
SLC9C282
SLC9C283
SLC9C284
SLC9C285
SLC9C286
SLC9C287
SLC9C288
SLC9C289
SLC9C290
SLC9C291
SLC9C292
SLC9C293
SLC9C294
SLC9C295
SLC9C296
SLC9C297
SLC9C298
SLC9C299
SLC9C300
SLC9C301
SLC9C302
SLC9C303
SLC9C304
SLC9C305
SLC9C306
SLC9C307
SLC9C308
SLC9C309
SLC9C310
SLC9C311
SLC9C312
SLC9C313
SLC9C314
SLC9C315
SLC9C316
SLC9C317
SLC9C318
SLC9C319
SLC9C320
SLC9C321
SLC9C322
SLC9C323
SLC9C324
SLC9C325
SLC9C326
SLC9C327
SLC9C328
SLC9C329
SLC9C330
SLC9C331
SLC9C332
SLC9C333
SLC9C334
SLC9C335
SLC9C336
SLC9C337
SLC9C338
SLC9C339
SLC9C340
SLC9C341
SLC9C342
SLC9C343
SLC9C344
SLC9C345
SLC9C346
SLC9C347
SLC9C348
SLC9C349
SLC9C350
SLC9C351
SLC9C352
SLC9C353
SLC9C354
SLC9C355
SLC9C356
SLC9C357
SLC9C358
SLC9C359
SLC9C360
SLC9C361
SLC9C362
SLC9C363
SLC9C364
SLC9C365
SLC9C366
SLC9C367
SLC9C368
SLC9C369
SLC9C370
SLC9C371
SLC9C372
SLC9C373
SLC9C374
SLC9C375
SLC9C376
SLC9C377
SLC9C378
SLC9C379
SLC9C380
SLC9C381
SLC9C382
SLC9C383
SLC9C384
SLC9C385
SLC9C386
SLC9C387
SLC9C388
SLC9C389
SLC9C390
SLC9C391
SLC9C392
SLC9C393
SLC9C394
SLC9C395
SLC9C396
SLC9C397
SLC9C398
SLC9C399
SLC9C400
SLC9C401
SLC9C402
SLC9C403
SLC9C404
SLC9C405
SLC9C406
SLC9C407
SLC9C408
SLC9C409
SLC9C410
SLC9C411
SLC9C412
SLC9C413
SLC9C414
SLC9C415
SLC9C416
SLC9C417
SLC9C418
SLC9C419
SLC9C420
SLC9C421
SLC9C422
SLC9C423
SLC9C424
SLC9C425
SLC9C426
SLC9C427
SLC9C428
SLC9C429
SLC9C430
SLC9C431
SLC9C432
SLC9C433
SLC9C434
SLC9C435
SLC9C436
SLC9C437
SLC9C438
SLC9C439
SLC9C440
SLC9C441
SLC9C442
SLC9C443
SLC9C444
SLC9C445
SLC9C446
SLC9C447
SLC9C448
SLC9C449
SLC9C450
SLC9C451
SLC9C452
SLC9C453
SLC9C454
SLC9C455
SLC9C456
SLC9C457
SLC9C458
SLC9C459
SLC9C460
SLC9C461
SLC9C462
SLC9C463
SLC9C464
SLC9C465
SLC9C466
SLC9C467
SLC9C468
SLC9C469
SLC9C470
SLC9C471
SLC9C472
SLC9C473
SLC9C474
SLC9C475
SLC9C476
SLC9C477
SLC9C478
SLC9C479
SLC9C480
SLC9C481
SLC9C482
SLC9C483
SLC9C484
SLC9C485
SLC9C486
SLC9C487
SLC9C488
SLC9C489
SLC9C490
SLC9C491
SLC9C492
SLC9C493
SLC9C494
SLC9C495
SLC9C496
SLC9C497
SLC9C498
SLC9C499
SLC9C500
SLC9C501
SLC9C502
SLC9C503
SLC9C504
SLC9C505
SLC9C506
SLC9C507
SLC9C508
SLC9C509
SLC9C510
SLC9C511
SLC9C512
SLC9C513
SLC9C514
SLC9C515
SLC9C516
SLC9C517
SLC9C518
SLC9C519
SLC9C520
SLC9C521
SLC9C522
SLC9C523
SLC9C524
SLC9C525
SLC9C526
SLC9C527
SLC9C528
SLC9C529
SLC9C530
SLC9C531
SLC9C532
SLC9C533
SLC9C534
SLC9C535
SLC9C536
SLC9C537
SLC9C538
SLC9C539
SLC9C540
SLC9C541
SLC9C542
SLC9C543
SLC9C544
SLC9C545
SLC9C546
SLC9C547
SLC9C548
SLC9C549
SLC9C550
SLC9C551
SLC9C552
SLC9C553
SLC9C554
SLC9C555
SLC9C556
SLC9C557
SLC9C558
SLC9C559
SLC9C560
SLC9C561
SLC9C562
SLC9C563
SLC9C564
SLC9C565
SLC9C566
SLC9C567
SLC9C568
SLC9C569
SLC9C570
SLC9C571
SLC9C572
SLC9C573
SLC9C574
SLC9C575
SLC9C576
SLC9C577
SLC9C578
SLC9C579
SLC9C580
SLC9C581
SLC9C582
SLC9C583
SLC9C584
SLC9C585
SLC9C586
SLC9C587
SLC9C588
SLC9C589
SLC9C590
SLC9C591
SLC9C592
SLC9C593
SLC9C594
SLC9C595
SLC9C596
SLC9C597
SLC9C598
SLC9C599
SLC9C600
SLC9C601
SLC9C602
SLC9C603
SLC9C604
SLC9C605
SLC9C606
SLC9C607
SLC9C608
SLC9C609
SLC9C610
SLC9C611
SLC9C612
SLC9C613
SLC9C614
SLC9C615
SLC9C616
SLC9C617
SLC9C618
SLC9C619
SLC9C620
SLC9C621
SLC9C622
SLC9C623
SLC9C624
SLC9C625
SLC9C626
SLC9C627
SLC9C628
SLC9C629
SLC9C630
SLC9C631
SLC9C632
SLC9C633
SLC9C634
SLC9C635
SLC9C636
SLC9C637
SLC9C638
SLC9C639
SLC9C640
SLC9C641
SLC9C642
SLC9C643
SLC9C644
SLC9C645
SLC9C646
SLC9C647
SLC9C648
SLC9C649
SLC9C650
SLC9C651
SLC9C652
SLC9C653
SLC9C654
SLC9C655
SLC9C656
SLC9C657
SLC9C658
SLC9C659
SLC9C660
SLC9C661
SLC9C662
SLC9C663
SLC9C664
SLC9C665
SLC9C666
SLC9C667
SLC9C668
SLC9C669
SLC9C670
SLC9C671
SLC9C672
SLC9C673
SLC9C674
SLC9C675
SLC9C676
SLC9C677
SLC9C678
SLC9C679
SLC9C680
SLC9C681
SLC9C682
SLC9C683
SLC9C684
SLC9C685
SLC9C686
SLC9C687
SLC9C688
SLC9C689
SLC9C690
SLC9C691
SLC9C692
SLC9C693
SLC9C694
SLC9C695
SLC9C696
SLC9C697
SLC9C698
SLC9C699
SLC9C700
SLC9C701
SLC9C702
SLC9C703
SLC9C704
SLC9C705
SLC9C706
SLC9C707
SLC9C708
SLC9C709
SLC9C710
SLC9C711
SLC9C712
SLC9C713
SLC9C714
SLC9C715
SLC9C716
SLC9C717
SLC9C718
SLC9C719
SLC9C720
SLC9C721
SLC9C722
SLC9C723
SLC9C724
SLC9C725
SLC9C726
SLC9C727
SLC9C728
SLC9C729
SLC9C730
SLC9C731
SLC9C732
SLC9C733
SLC9C734
SLC9C735
SLC9C736
SLC9C737
SLC9C738
SLC9C739
SLC9C740
SLC9C741
SLC9C742
SLC9C743
SLC9C744
SLC9C745
SLC9C746
SLC9C747
SLC9C748
SLC9C749
SLC9C750
SLC9C751
SLC9C752
SLC9C753
SLC9C754
SLC9C755
SLC9C756
SLC9C757
SLC9C758
SLC9C759
SLC9C760
SLC9C761
SLC9C762
SLC9C763
SLC9C764
SLC9C765
SLC9C766
SLC9C767
SLC9C768
SLC9C769
SLC9C770
SLC9C771
SLC9C772
SLC9C773
SLC9C774
SLC9C775
SLC9C776
SLC9C777
SLC9C778
SLC9C779
SLC9C780
SLC9C781
SLC9C782
SLC9C783
SLC9C784
SLC9C785
SLC9C786
SLC9C787
SLC9C788
SLC9C789
SLC9C790
SLC9C791
SLC9C792
SLC9C793
SLC9C794
SLC9C795
SLC9C796
SLC9C797
SLC9C798
SLC9C799
SLC9C800
SLC9C801
SLC9C802
SLC9C803
SLC9C804
SLC9C805
SLC9C806
SLC9C807
SLC9C808
SLC9C809
SLC9C810
SLC9C811
SLC9C812
SLC9C813
SLC9C814
SLC9C815
SLC9C816
SLC9C817
SLC9C818
SLC9C819
SLC9C820
SLC9C821
SLC9C822
SLC9C823
SLC9C824
SLC9C825
SLC9C826
SLC9C827
SLC9C828
SLC9C829
SLC9C830
SLC9C831
SLC9C832
SLC9C833
SLC9C834
SLC9C835
SLC9C836
SLC9C837
SLC9C838
SLC9C839
SLC9C840
SLC9C841
SLC9C842
SLC9C843
SLC9C844
SLC9C845
SLC9C846
SLC9C847
SLC9C848
SLC9C849
SLC9C850
SLC9C851
SLC9C852
SLC9C853
SLC9C854
SLC9C855
SLC9C856
SLC9C857
SLC9C858
SLC9C859
SLC9C860
SLC9C861
SLC9C862
SLC9C863
SLC9C864
SLC9C865
SLC9C866
SLC9C867
SLC9C868
SLC9C869
SLC9C870
SLC9C871
SLC9C872
SLC9C873
SLC9C874
SLC9C875
SLC9C876
SLC9C877
SLC9C878
SLC9C879
SLC9C880
SLC9C881
SLC9C882
SLC9C883
SLC9C884
SLC9C885
SLC9C886
SLC9C887
SLC9C888
SLC9C889
SLC9C890
SLC9C891
SLC9C892
SLC9C893
SLC9C894
SLC9C895
SLC9C896
SLC9C897
SLC9C898
SLC9C899
SLC9C900
SLC9C901
SLC9C902
SLC9C903
SLC9C904
SLC9C905
SLC9C906
SLC9C907
SLC9C908
SLC9C909
SLC9C910
SLC9C911
SLC9C912
SLC9C913
SLC9C914
SLC9C915
SLC9C916
SLC9C917
SLC9C918
SLC9C919
SLC9C920
SLC9C921
SLC9C922
SLC9C923
SLC9C924
SLC9C925
SLC9C926
SLC9C927
SLC9C928
SLC9C929
SLC9C930
SLC9C931
SLC9C932
SLC9C933
SLC9C934
SLC9C935
SLC9C936
SLC9C937
SLC9C938
SLC9C939
SLC9C940
SLC9C941
SLC9C942
SLC9C943
SLC9C944
SLC9C945
SLC9C946
SLC9C947
SLC9C948
SLC9C949
SLC9C950
SLC9C951
SLC9C952
SLC9C953
SLC9C954
SLC9C955
SLC9C956
SLC9C957
SLC9C958
SLC9C959
SLC9C960
SLC9C961
SLC9C962
SLC9C963
SLC9C964
SLC9C965
SLC9C966
SLC9C967
SLC9C968
SLC9C969
SLC9C970
SLC9C971
SLC9C972
SLC9C973
SLC9C974
SLC9C975
SLC9C976
SLC9C977
SLC9C978
SLC9C979
SLC9C980
SLC9C981
SLC9C982
SLC9C983
SLC9C984
SLC9C985
SLC9C986
SLC9C987
SLC9C988
SLC9C989
SLC9C990
SLC9C991
SLC9C992
SLC9C993
SLC9C994
SLC9C995
SLC9C996
SLC9C997
SLC9C998
SLC9C999
SLC9C1000
SLC9C1001
SLC9C1002
SLC9C1003
SLC9C1004
SLC9C1005
SLC9C1006
SLC9C1007
SLC9C1008
SLC9C1009
SLC9C1010
SLC9C1011
SLC9C1012
SLC9C1013
SLC9C1014
SLC9C1015
SLC9C1016
SLC9C1017
SLC9C1018
SLC9C1019
SLC9C1020
SLC9C1021
SLC9C1022
SLC9C1023
SLC9C1024
SLC9C1025
SLC9C1026
SLC9C1027
SLC9C1028
SLC9C1029
SLC9C1030
SLC9C1031
SLC9C1032
SLC9C1033
SLC9C1034
SLC9C1035
SLC9C1036
SLC9C1037
SLC9C1038
SLC9C1039
SLC9C1040
SLC9C1041
SLC9C1042
SLC9C1043
SLC9C1044
SLC9C1045
SLC9C1046
SLC9C1047
SLC9C1048
SLC9C1049
SLC9C1050
SLC9C1051
SLC9C1052
SLC9C1053
SLC9C1054
SLC9C1055
SLC9C1056
SLC9C1057
SLC9C1058
SLC9C1059
SLC9C1060
SLC9C1061
SLC9C1062
SLC9C1063
SLC9C1064
SLC9C1065
SLC9C1066
SLC9C1067
SLC9C1068
SLC9C1069
SLC9C1070
SLC9C1071
SLC9C1072
SLC9C1073
SLC9C1074
SLC9C1075
SLC9C1076
SLC9C1077
SLC9C1078
SLC9C1079
SLC9C1080
SLC9C1081
SLC9C1082
SLC9C1083
SLC9C1084
SLC9C1085
SLC9C1086
SLC9C1087
SLC9C1088
SLC9C1089
SLC9C1090
SLC9C1091
SLC9C1092
SLC9C1093
SLC9C1094
SLC9C1095
SLC9C1096
SLC9C1097
SLC9C1098
SLC9C1099
SLC9C1100
SLC9C1101
SLC9C1102
SLC9C1103
SLC9C1104
SLC9C1105
SLC9C1106
SLC9C1107
SLC9C1108
SLC9C1109
SLC9C1110
SLC9C1111
SLC9C1112
SLC9C1113
SLC9C1114
SLC9C1115
SLC9C1116
SLC9C1117
SLC9C1118
SLC9C1119
SLC9C1120
SLC9C1121
SLC9C1122
SLC9C1123
SLC9C1124
SLC9C1125
SLC9C1126
SLC9C1127
SLC9C1128
SLC9C1129
SLC9C1130
SLC9C1131
SLC9C1132
SLC9C1133
SLC9C1134
SLC9C1135
SLC9C1136
SLC9C1137
SLC9C1138
SLC9C1139
SLC9C1140
SLC9C1141
SLC9C1142
SLC9C1143
SLC9C1144
SLC9C1145
SLC9C1146
SLC9C1147
SLC9C1148
SLC9C1149
SLC9C1150
SLC9C1151
SLC9C1152
SLC9C1153
SLC9C1154
SLC9C1155
SLC9C1156
SLC9C1157
SLC9C1158
SLC9C1159
SLC9C1160
SLC9C1161
SLC9C1162
SLC9C1163
SLC9C1164
SLC9C1165
SLC9C1166
SLC9C1167
SLC9C1168
SLC9C1169
SLC9C1170
SLC9C1171
SLC9C1172
SLC9C1173
SLC9C1174
SLC9C1175
SLC9C1176
SLC9C1177
SLC9C1178
SLC9C1179
SLC9C1180
SLC9C1181
SLC9C1182
SLC9C1183
SLC9C1184
SLC9C1185
SLC9C1186
SLC9C1187
SLC9C1188
SLC9C1189
SLC9C1190
SLC9C1191
SLC9C1192
SLC9C1193
SLC9C1194
SLC9C1195
SLC9C1196
SLC9C1197
SLC9C1198
SLC9C1199
SLC9C1200
SLC9C1201
SLC9C1202
SLC9C1203
SLC9C1204
SLC9C1205
SLC9C1206
SLC9C1207
SLC9C1208
SLC9C1209
SLC9C1210
SLC9C1211
SLC9C1212
SLC9C1213
SLC9C1214
SLC9C1215
SLC9C1216
SLC9C1217
SLC9C1218
SLC9C1219
SLC9C1220
SLC9C1221
SLC9C1222
SLC9C1223
SLC9C1224
SLC9C1225
SLC9C1226
SLC9C1227
SLC9C1228
SLC9C1229
SLC9C1230
SLC9C1231
SLC9C1232
SLC9C1233
SLC9C1234
SLC9C1235
SLC9C1236
SLC9C1237
SLC9C1238
SLC9C1239
SLC9C1240
SLC9C1241
SLC9C1242
SLC9C1243
SLC9C1244
SLC9C1245
SLC9C1246
SLC9C1247
SLC9C1248
SLC9C1249
SLC9C1250
SLC9C1251
SLC9C1252
SLC9C1253
SLC9C1254
SLC9C1255
SLC9C1256
SLC9C1257
SLC9C1258
SLC9C1259
SLC9C1260
SLC9C1261
SLC9C1262
SLC9C1263
SLC9C1264
SLC9C1265
SLC9C1266
SLC9C1267
SLC9C1268
SLC9C1269
SLC9C1270
SLC9C1271
SLC9C1272
SLC9C1273
SLC9C1274
SLC9C1275
SLC9C1276
SLC9C1277
SLC9C1278
SLC9C1279
SLC9C1280
SLC9C1281
SLC9C1282
SLC9C1283
SLC9C1284
SLC9C1285
SLC9C1286
SLC9C1287
SLC9C1288
SLC9C1289
SLC9C1290
SLC9C1291
SLC9C1292
SLC9C1293
SLC9C1294
SLC9C1295
SLC9C1296
SLC9C1297
SLC9C1298
SLC9C1299
SLC9C1300
SLC9C1301
SLC9C1302
SLC9C1303
SLC9C1304
SLC9C1305
SLC9C1306
SLC9C1307
SLC9C1308
SLC9C1309
SLC9C1310
SLC9C1311
SLC9C1312
SLC9C1313
SLC9C1314
SLC9C1315
SLC9C1316
SLC9C1317
SLC9C1318
SLC9C1319
SLC9C1320
SLC9C1321
SLC9C1322
SLC9C1323
SLC9C1324
SLC9C1325
SLC9C1326
SLC9C1327
SLC9C1328
SLC9C1329
SLC9C1330
SLC9C1331
SLC9C1332
SLC9C1333
SLC9C1334
SLC9C1335
SLC9C1336
SLC9C1337
SLC9C1338
SLC9C1339
SLC9C1340
SLC9C1341
SLC9C1342
SLC9C1343
SLC9C1344
SLC9C1345
SLC9C1346
SLC9C1347
SLC9C1348
SLC9C1349
SLC9C1350
SLC9C1351
SLC9C1352
SLC9C1353
SLC9C1354
SLC9C1355
SLC9C1356
SLC9C1357
SLC9C1358
SLC9C1359
SLC9C1360
SLC9C1361
SLC9C1362
SLC9C1363
SLC9C1364
SLC9C1365
SLC9C1366
SLC9C1367
SLC9C1368
SLC9C1369
SLC9C1370
SLC9C1371
SLC9C1372
SLC9C1373
SLC9C1374
SLC9C1375
SLC9C1376
SLC9C1377
SLC9C1378
SLC9C1379
SLC9C1380
SLC9C1381
SLC9C1382
SLC9C1383
SLC9C1384
SLC9C1385
SLC9C1386
SLC9C1387
SLC9C1388
SLC9C1389
SLC9C1390
SLC9C1391
SLC9C1392
SLC9C1393
SLC9C1394
SLC9C1395
SLC9C1396
SLC9C1397
SLC9C1398
SLC9C1399
SLC9C1400
SLC9C1401
SLC9C1402
SLC9C1403
SLC9C1404
SLC9C1405
SLC9C1406
SLC9C1407
SLC9C1408
SLC9C1409
SLC9C1410
SLC9C1411
SLC9C1412
SLC9C1413
SLC9C1414
SLC9C1415
SLC9C1416
SLC9C1417
SLC9C1418
SLC9C1419
SLC9C1420
SLC9C1421
SLC9C1422
SLC9C1423
SLC9C1424
SLC9C1425
SLC9C1426
SLC9C1427
SLC9C1428
SLC9C1429
SLC9C1430
SLC9C1431
SLC9C1432
SLC9C1433
SLC9C1434
SLC9C1435
SLC9C1436
SLC9C1437
SLC9C1438
SLC9C1439
SLC9C1440
SLC9C1441
SLC9C1442
SLC9C1443
SLC9C1444
SLC9C1445
SLC9C1446
SLC9C1447
SLC9C1448
SLC9C1449
SLC9C1450
SLC9C1451
SLC9C1452
SLC9C1453
SLC9C1454
SLC9C1455
SLC9C1456
SLC9C1457
SLC9C1458
SLC9C1459
SLC9C1460
SLC9C1461
SLC9C1462
SLC9C1463
SLC9C1464
SLC9C1465
SLC9C1466
SLC9C1467
SLC9C1468
SLC9C1469
SLC9C1470
SLC9C1471
SLC9C1472
SLC9C1473
SLC9C1474
SLC9C1475
SLC9C1476
SLC9C1477
SLC9C1478
SLC9C1479
SLC9C1480
SLC9C1481
SLC9C1482
SLC9C1483
SLC9C1484
SLC9C1485
SLC9C1486
SLC9C1487
SLC9C1488
SLC9C1489
SLC9C1490
SLC9C1491
SLC9C1492
SLC9C1493
SLC9C1494
SLC9C1495
SLC9C1496
SLC9C1497
SLC9C1498
SLC9C1499
SLC9C1500
SLC9C1501
SLC9C1502
SLC9C1503
SLC9C1504
SLC9C1505
SLC9C1506
SLC9C1507
SLC9C1508
SLC9C1509
SLC9C1510

TUBA4B
TUBA8
TUBA1C
TUBA4A
TUBGCP5
TTC21A
TTC30B
TTC29B
TTC29A
TTL3
TUBB4B
TUBB3B
TMX4
TMX3B
TYW3B
UBA1B
UBA1D
UBA1E
UBC9B
USP2
USP25
USMP1
VAS1B
VASN
VASP
VIPAS
VIPR1
VT
VSMC11
VMA21
VNN2
VSNL1
WAS3
WASF1
WDR1
WDR4
WDR18
WFS1
WNT11
WRN
WPC
XPC
YIPF1
YRDC
YPEL2
ZBTB12
ZBTB42
ZBTB7C
ZBTB7C
ZCCHC18
ZCCHC24
ZFAND4
ZFP69B
ZNF410
ZNF516
ZNF580A
ZNF593
ZNF712
ZNEF1
ZPR
ZSCAN9
ZS